Comparing glacial and Holocene opal fluxes in the Pacific sector of the Southern Ocean

Louisa I. Bradtmiller,[1,2,3] Robert F. Anderson,[1,2] Martin Q. Fleisher,[1] and Lloyd H. Burckle[1]

Received 30 September 2008; revised 19 February 2009; accepted 25 March 2009; published 3 June 2009.

[1] The silicic acid leakage hypothesis (SALH) predicts that during glacial periods excess silicic acid was transported from the Southern Ocean to lower latitudes, which favored diatom production over coccolithophorid production and caused a drawdown of atmospheric CO_2. Downcore records of ^{230}Th-normalized opal (biogenic silica) fluxes from 31 cores in the Pacific sector of the Southern Ocean were used to compare diatom productivity during the last glacial period to that of the Holocene and to examine the evidence for increased glacial Si export to the tropics. Average glacial opal fluxes south of the modern Antarctic Polar Front (APF) were less than during the Holocene, while average glacial opal fluxes north of the APF were greater than during the Holocene. However, the magnitude of the increase north of the APF was not enough to offset decreased fluxes to the south, resulting in a decrease in opal burial in the Pacific sector of the Southern Ocean during the last glacial period, equivalent to approximately 15 Gt opal ka^{-1}. This is consistent with the work of Chase et al. (2003a), and satisfies the primary requirement of the SALH, assuming that the upwelled supply of Si was approximately equivalent during the Holocene and the glacial period. However, previous results from the equatorial oceans are inconsistent with the other predictions of the SALH, namely that either the C_{org}:$CaCO_3$ ratio or the rate of opal burial should have increased during glacial periods. We compare the magnitudes of changes in the Southern Ocean and the tropics and suggest that Si escaping the glacial Southern Ocean must have had an alternate destination, possibly the continental margins. There is currently insufficient data to test this hypothesis, but the existence of this sink and its potential impact on glacial pCO_2 remain interesting topics for future study.

Citation: Bradtmiller, L. I., R. F. Anderson, M. Q. Fleisher, and L. H. Burckle (2009), Comparing glacial and Holocene opal fluxes in the Pacific sector of the Southern Ocean, *Paleoceanography*, *24*, PA2214, doi:10.1029/2008PA001693.

1. Introduction

[2] Changes in Earth's climate, including air temperature and deep-sea temperature, have been associated with changes in the concentration of carbon dioxide and other greenhouse gasses in the atmosphere [*Shackleton*, 2000]. Interglacial periods during the past 400,000 years (including the preindustrial period) were characterized by pCO_2 levels of approximately 280 ppm, while pCO_2 during peak glacial conditions ranged from 180 to 200 ppm [*Petit et al.*, 1999; *Siegenthaler et al.*, 2005]. It is widely held that changes in atmospheric CO_2 content are linked to climate through the ocean carbon cycle, because of its reservoir size (approximately 50X the size of the atmospheric carbon reservoir) and rate of overturning (~1500 years for the deep ocean) [*Broecker et al.*, 2004]. However, specific mechanisms to explain this link have yet to be identified [*Archer et al.*, 2000; *Peacock et al.*, 2006; *Sigman and Boyle*, 2000]. Given that cumulative anthropogenic CO_2 input to the atmosphere (100 ppm) (P. Tans, Trends in carbon dioxide, 2008, available at www.esrl.noaa.gov/gmd/ccgg/trends/) now equals the magnitude of natural variability over the past several glacial cycles, and that the input of anthropogenic CO_2 is likely to continue increasing, there is intense interest among scientists and the general public in understanding the causes of natural CO_2 variability, with expectations that doing so will improve predictions of the ocean's uptake of anthropogenic CO_2 in the future.

[3] The Silicic Acid Leakage Hypothesis (SALH) [*Brzezinski et al.*, 2002; *Matsumoto et al.*, 2002b] seeks to explain a portion of glacial-interglacial CO_2 variability through changes in the ocean silicon cycle. The SALH suggests that during glacial periods the fraction of upwelled silicic acid ($Si(OH)_4$) utilized by diatoms in the Southern Ocean (SO) was less than during interglacials. The excess (i.e., unused) Si was then incorporated into Subantarctic Mode Water (SAMW) and transported through the thermocline to low-latitude upwelling zones (where diatoms are presently Si limited). It has been shown that in the presence of sufficient Si, diatoms can outcompete other taxa for nitrogen and phosphorus [*Dugdale and Wilkerson*, 1998], which are relatively abundant in the modern tropics. The addition of Si to the tropics would therefore have increased diatom productivity at the expense of other taxa, including coccolithophorids leading to decreased $CaCO_3$ production and a corresponding rise in ocean alkalinity due to $CaCO_3$

[1]Lamont-Doherty Earth Observatory of Columbia University, Palisades, New York, USA.
[2]Also at Department of Earth and Environmental Sciences, Columbia University, New York, New York, USA.
[3]Now at Department of Marine Chemistry and Geochemistry, Woods Hole Oceanographic Institution, Woods Hole, Massachusetts, USA.

0883-8305/09/2008PA001693$12.00

compensation. A box model simulation of SALH conditions found that the combined effects of reducing carbonate production at the sea surface and carbonate compensation in the deep ocean would reduce glacial pCO_2 by 40–50 ppm [*Matsumoto et al.*, 2002b]. Previous tests of the SALH and more detailed discussions of the basic principles involved can be found in a number of earlier studies [e.g., *Bradtmiller et al.*, 2006, 2007; *Brzezinski et al.*, 2002; *S. S. Kienast et al.*, 2006; *Matsumoto et al.*, 2002b; *Sarmiento et al.*, 2004]. We present new sedimentary evidence from the Pacific sector of the Southern Ocean to test the SALH prediction that biogenic silica (opal) burial rates should have been less during the Last Glacial Period (LGP) than today.

2. Background

[4] The SALH is based on the premise that more Si escaped the glacial Southern Ocean than today, and that this Si arrived in the tropics through mode water circulation. The goal here is to compare Holocene and glacial opal burial rates in Southern Ocean sediments as a test of the SALH. Before presenting the results, it is appropriate to consider first the assumptions inherent in this approach and to review past studies that have provided relevant data.

2.1. Assumptions

[5] The SALH, and any tests of the SALH, must operate under a number of assumptions about continental weathering, ocean circulation and the oceanic Si cycle, among others. Both alkalinity and dissolved Si are supplied to the ocean through continental weathering, and the SALH makes the explicit assumption that the supply of both was constant over the past glacial cycle [*Brzezinski et al.*, 2002]. *Foster and Vance* [2006] made the case for this assumption using lead isotopes, concluding that the decrease in chemical weathering of the North American interior during the cold, dry glacial period was roughly balanced by the increase in chemical weathering of the newly exposed continental shelves. *Hammond et al.* [2004] came to a similar conclusion using the Ge/Si ratio of the ocean over time, constraining the global silicate weathering rate during the last glacial maximum to 106 ± 16% of the modern value. While this and other evidence suggests that total weathering rates remained roughly the same throughout the last glacial cycle, it is nevertheless important to keep this assumption in mind when testing the SALH.

[6] Even if the glacial oceanic inventory of Si were equal to that of the Holocene, it would still be possible to change local burial rates through changes in ocean circulation. Stronger upwelling in the Antarctic Circumpolar Current (ACC) could provide more Si to the surface SO, leading to enhanced productivity and greater opal burial, assuming that diatoms utilize all available Si as they do today [*Sigmon et al.*, 2002]. The reverse scenario also applies. Therefore, in testing the SALH by measuring opal burial rates in the Southern Ocean, one must assume equal rates of upwelling during the LGP and the Holocene, although not necessarily during the periods in between (i.e., the deglacial period). There is a great deal of contradictory evidence in this regard, much of which has been summarized by *Anderson et al.* [2002]. Some studies invoke decreased glacial upwelling south of the APF on the basis of proposed northward movement of the mean position of the westerlies [*Francois et al.*, 1997; *Sigman and Boyle*, 2000]. However, *Anderson et al.* [2002] point out that this is inconsistent with other evidence for poleward movement of the westerlies during the glacial period [*Valdes*, 2000], and also with evidence that the mean position of the APF remained relatively constant over the last glacial cycle [*Matsumoto et al.*, 2001]. This view is also supported by the approximately equal rates of opal burial in the Atlantic and Indian sectors of the SO during the LGP and the Holocene (see below). The conclusion of Anderson et al., and the assumption of this study, is that the mean position of the APF and the overall rate of Si supply by upwelling were not drastically different during the LGP than today.

[7] Finally, in order to test the SALH, the rate of opal dissolution must be assumed to be relatively constant. Opal dissolution is affected by the rate of opal production (i.e., bloom versus nonbloom environment), the sinking rate through the water column and water temperature, among many other factors [*Nelson et al.*, 1995]. It is not possible to reconstruct ecosystem dynamics in the glacial southern ocean, and so the first two must be assumed to have been constant. Colder ocean temperatures (both at the surface and in the deep ocean) may have slightly enhanced opal preservation during the LGP, although the uncertainty of glacial temperature estimates makes this difficult to quantify. However, no available estimates of Southern Ocean LGP-Holocene temperature change approach the 15°C needed to change the opal dissolution rate by an order of magnitude [*Hurd and Birdwhistell*, 1983; *Kamatani*, 1982]. A study in the eastern equatorial Pacific Ocean concluded that there has been little change in opal preservation over the last glacial cycle [*Warnock et al.*, 2007], which can be interpreted to mean that the overall state of ocean undersaturation with respect to Si was similar to today, although local variability cannot be ruled out. Last, it has been pointed out that differing susceptibility to dissolution among SO diatom species may alter the fraction of opal flux that is preserved [*Abelmann et al.*, 2006], so variable preservation must be considered when interpreting opal fluxes.

2.2. Prior Studies

[8] With the assumption of a constant rate of upwelling and supply of dissolved Si to SO surface waters, the SALH predicts that total opal burial rates in SO sediments would have been lower during the LGP than the Holocene. A number of studies have reconstructed opal burial in all three sectors of the Southern Ocean, and data from the Atlantic and Indian sectors of the SO show decreased glacial opal flux (relative to the Holocene) south of the Antarctic Polar Front (APF), as predicted by the SALH (the APF is defined as the northernmost limit of water with a minimum temperature less than 2°C at 200 m; in other words, the northernmost limit of upwelling [*Trull et al.*, 2001]). However, this decrease appears to have been offset by increased opal flux north of the APF, resulting in no net glacial-interglacial change in either sector [*Chase et al.*, 2003a; *Dezileau et al.*, 2003; *Diekmann*, 2007; *Francois et al.*, 1997; *Frank et al.*, 2000; *Kumar et al.*, 1995].

Table 1. Location and Water Depth of the Cores Used in This Study

Core	Latitude	Longitude	Water Depth	APF Position[a]
E11-3	−56.90	−115.24	4023	5.29
E11-4	−57.83	−115.22	4774	4.37
E11-7	−60.92	−114.78	5029	1.28
E11-12	−65.87	−115.08	4718	−3.67
E14-16	−58.99	−125.03	4499	1.28
E14-17	−57.83	−124.95	3904	2.44
E15-4	−59.02	−99.76	4910	2.29
E15-5	−58.02	−99.98	4307	3.29
E15-6	−59.97	−101.32	4517	0.91
E15-12	−58.68	−108.80	4572	3.00
E15-14	−58.06	−120.14	4255	2.30
E15-28	−56.02	−149.82	3328	−0.14
E17-7	−61.08	−134.35	4435	−2.58
E19-6	−61.93	−107.96	5064	−0.23
E19-7	−62.16	−109.09	5051	−0.48
E20-13	−55.00	−104.95	3895	4.83
E21-20	−60.25	−120.17	4701	0.11
E23-14	−63.82	−108.85	4957	−2.14
E23-17	−60.22	−114.63	5026	1.98
E23-18	−58.98	−115.00	5272	3.22
E25-16	−56.15	−156.22	3621	1.51
E27-23	−59.62	155.24	3182	−2.70
E33-19	−59.86	−119.66	4389	0.54
E36-36	−60.39	157.53	2816	−2.34
RC8-71	−58.05	155.73	3224	−0.87
V16-115	−55.68	141.28	3147	0.01
V16-121	−50.67	164.38	3614	9.41
V17-88TW	−57.03	−74.48	4063	6.42
V17-90	−60.13	−74.93	4568	3.33
V18-73TW	−61.53	−73.28	4568	1.31
V18-93	−59.48	−64.78	3834	−0.17
E11-2[b]	−56.07	−115.09	3111	6.00
E14-5[b]	−56.20	−160.53	4015	2.80
E14-6[b]	−57.01	−160.15	4517	2.00
E17-9[b]	−63.08	−135.08	4849	−4.50
E20-10[b]	−60.22	−127.05	4474	0.00
E33-22[b]	−54.93	−120.00	2744	7.00
NBP9802-3[b,c]	−66.14	−169.49		−5.88
NBP9802-4[b,c]	−64.20	−170.08		−3.95
NBP9802-5[b,c]	−63.17	−169.85		−2.86
NBP9802-6[b,c]	−61.87	−169.97		−1.63
NBP9802-7[b,c]	−60.24	−170.19		0.00
NBP9802-8[b,c]	−58.69	−169.98		1.55
NBP9802-9[b,c]	−56.94	−170.23		3.35
NBP9802-10[b,c]	−53.04	−174.69		7.25

[a]APF position reflects position of cores expressed as degrees north of the APF as defined by *Orsi et al.* [1995].
[b]Cores and data from *Chase et al.* [2003a].
[c]Includes multiple cores per site (multicores, piston cores, and gravity cores) at different depths; see *Chase et al.* [2003a] for depths of all cores.

[9] Opal flux data from the Pacific sector show a glacial decrease south of the APF similar in magnitude to the other sectors, but only a very slight increase north of the APF [*Chase et al.*, 2003a], suggesting lower total glacial opal burial. If Si supply was similar to today, this may indicate reduced Si consumption in the Pacific sector of the glacial SO, and therefore allow for increased export of dissolved Si to the tropics. However, the Chase et al. results were based on a relatively small number of cores given the large area of the Pacific sector of the Southern Ocean, and core locations were primarily concentrated into a few areas. Therefore, we undertook a study of 31 additional cores over a wider geographical range in order to better constrain changes in LGP opal burial and, by inference, Si export from the Pacific sector of the Southern Ocean.

3. Core Selection and Age Models

[10] Over 350 cores were originally considered for this project, comprising all cores in the Pacific sector of the Southern Ocean archived at the LDEO and Antarctic Research Facility (ARF at Florida State University) repositories meeting the following criteria: (1) south of the subtropical front, (2) north of a boundary set at 5° south of the APF and (3) greater than 1000 m water depth. Core descriptions archived at the ARF facility and direct observation of the cores enabled us to reduce the number of candidate cores to 127. This section provides a brief overview of the overall strategy used to narrow the study to the 31 cores for which results are reported here. A more detailed discussion about how multiple proxies were used to constrain age models can be found in the Appendix. Complete latitude, longitude, relative APF position and depth data for these cores can be found in Table 1.

[11] It is particularly difficult to establish age models in Southern Ocean cores using the methods employed in most of the rest of the ocean. This is partially due to sediment scouring and redistribution by strong bottom currents, which enhance the possibility of a hiatus in any given core. Mostly, however, it is due to the low rates of production and poor preservation of $CaCO_3$ [*Howard and Prell*, 1992, 1994]. While traditional age models rely on ^{14}C dating and $\delta^{18}O$ of carbonate, the low carbonate content of the Southern Ocean forces us to look toward other methods to constrain both glacial-interglacial cycles and absolute ages. Radiocarbon measurements were made when possible, and all cores were studied using a more complex multistep strategy, outlined below.

[12] Briefly, as an initial assessment, magnetic susceptibility was used to identify potential glacial-interglacial cycles. South of the APF, high magnetic susceptibility identifies glacial periods, and low-susceptibility interglacials (see below). North of the APF, this is often (but not always) true. Microscopic slides were also examined (L. H. Burckle, unpublished data, 2003, 2005) at this time for *Hemidiscus karstenii,* a diatom species whose last abundance appearance datum corresponds with the top of isotope stage 7 [*Burckle et al.*, 1978], in order to eliminate cores missing late Pleistocene sediments. Remaining cores showing potential glacial-interglacial cycles were sampled for % *Eucampia antarctica*, in order to determine whether cycles evident in magnetic susceptibility records were in fact glacial-interglacial in nature [*Burckle and Cooke*, 1983; *Burckle and Burak*, 1995]. Cores with identified G-IG cycles were then sampled for % calcium carbonate, % opal and U/Th/Pa isotopic analyses. Carbonate minima can help to identify peak glacial periods, and % carbonate also helps to determine whether sufficient material exists for ^{14}C dating. Radiocarbon dating was used where possible to eliminate cores with age reversals and missing glacial cycles; these results can be found in Table 2. Finally, U series data were used to identify cores missing a full glacial cycle at the top of the record, as described in the online

Table 2. Radiocarbon Data From Cores Used in This Study[a]

Core	Depth (cm)	^{14}C Age (years)	σ	NOSAMS Number
E11-3	18	10,200	45	OS-62301
E11-3	48	26,400	170	OS-62305
E14-16	0–5	9,330	40	OS-62005
E14-16	30–35	13,900	130	OS-63291
E14-16	65	39,200	470	OS-63112
E14-16	73	40,000	380	OS-63114
E14-17	52	9,500	85	OS-62308
E14-17	82	13,450	55	OS-62306
E14-17	132–133	40,800	1300	OS-42056
E15-14	2	10,550	45	OS-62304
E15-14	92	34,400	230	OS-63115
E15-14	672	48,300	660	OS-63132
E15-14	672	38,700	1400	OS-63275
E15-28	5	8,690	80	OS-62207
E15-28	35	15,650	85	OS-62001
E15-5	30	8,090	45	OS-61989
E17-7	40	13,500	50	OS-62309
E20-13	15	11,050	60	OS-63134
E20-13	40	9,850	50	OS-62208
E20-13	60	24,700	580	OS-63294
E21-20	26	9,922	89	
E21-20	56	12,530	100	
E25-16	0	5,440	60	OS-62205
E25-16	25	11,100	50	OS-62204
E27-23	600–601	12,150	60	OS-51913
E27-23	740–741	14,300	65	OS-51910
E27-23	760–761	14,850	65	OS-51914
E27-23	780–781	18,250	95	OS-51915
E33-19	12	13,800	55	OS-62127
E33-19	42	9,970	55	OS-63116
E36-36	40	11,350	70	OS-63135
RC8-71	40	17,300	75	OS-51919
RC8-71	45–47	23,300	130	OS-51920
RC8-71	61–64	43,800	600	OS-63133
V16-115	67	10,050	45	OS-62206
V16-115	111–113	33,500	210	OS-51916
V16-115	134	25,900	440	OS-63283
V16-121	235–237	19,300	410	OS-52547
V18-93	15	9,610	55	OS-62209
V18-93	48–50	22,000	150	OS-51918
V18-93	65	27,300	150	OS-62210

[a]Radiocarbon measurements were performed at the National Ocean Sciences Accelerator Mass Spectrometry Facility (NOSAMS) using mixed species of planktonic foraminifera.

auxiliary material.[1] It should be emphasized that these methods of age control are solely intended to distinguish the LGM and surrounding interval, which we refer to as the LGP, from the Holocene; not to create a high-resolution downcore record with accurate age control points.

[13] After applying the techniques outlined above and described in detail in the online auxiliary material, the large majority of the 127 cores examined were discarded. The 31 remaining cores studied here range from 66°S to 50°S and 65°W to 220°W (see Figure 1). Nineteen of these are north of the APF [*Orsi et al.*, 1995], seven are south of the APF, and four lie within 0.2° of the APF. In the modern ocean, most opal burial takes place in the permanently open ocean zone to the south of the APF, with the polar frontal zone (the region between the APF and the Subantarctic front) being a secondary (and still significant) contributor [*Nelson et al.*, 2002].

4. Methods

[14] Uranium (^{238}U, ^{234}U), thorium (^{232}Th, ^{230}Th) and protactinium (^{231}Pa) concentrations were determined by isotope dilution using inductively coupled plasma mass spectrometry after sediment dissolution (HNO_3, HF and $HClO_4$ treatment) and anion resin column chemistry to separate the Pa fraction and U/Th fraction [*Anderson and Fleer*, 1982; *Fleisher and Anderson*, 2003]. Percent biogenic opal was measured by alkaline extraction after *Mortlock and Froelich* [1989]. Carbonate was measured by coulometry on a UIC CM5130 Acidification Module. Lithogenic (detrital) fluxes were calculated assuming a detrital source for all ^{232}Th, and an average detrital ^{232}Th content of 10 ppm for cores north of the APF [*Taylor and McLennan*, 1985] and 15 ppm for cores south of the APF. These values yield the closest sum to 100% when adding together the different sedimentary phases, and detrital U/Th measurements south of the APF are much lower than anywhere else in the world, consistent with higher ^{232}Th content. While it is fair to debate the use of different values north and south of the APF, it is important to remember that we are primarily interested in LGP-Holocene changes in detrital flux over the entire area of study. Because we use the same average detrital content for both the Holocene and the LGM within a given core, and because we are not attempting to interpret patterns of lithogenic flux north and south of the APF, we feel that this approach is justified and utilizes the best data available to the community. Magnetic susceptibility was measured using a Bartington meter with a point probe. Relative abundance of *E. antarctica* was based on the average of duplicate counts of no less than 300 diatoms per sample [*Burckle and Burak*, 1995]. Radiocarbon measurements were performed at the National Ocean Sciences Accelerator Mass Spectrometry Facility (NOSAMS) on mixed planktonic foraminifera tests. Samples for radiocarbon were disaggregated using distilled water, and sieved. The >250 μm size fraction was picked first, and supplemented by tests from the >150 μm size fraction when necessary.

[15] Opal, carbonate and detrital fluxes were calculated by normalizing to ^{230}Th to correct for lateral redistribution of sediments by deep-sea currents [*Bacon*, 1984; *Francois et al.*, 1990, 2004; *Frank et al.*, 1996]. Thorium normalization works on the assumption that the flux of particulate ^{230}Th sinking to the ocean floor is approximately equal to its known rate of production from ^{234}U decay in the water column because the residence time of ^{230}Th in the water column is relatively short (on the order of a few decades) [*Anderson et al.*, 1983b] compared to the timescale for lateral mixing in deep ocean basins [*Anderson et al.*, 1990]. Where burial rates of ^{230}Th are found to exceed its production in the water column, this is attributed to the lateral redistribution of sediments by deep-sea currents. The ^{230}Th normalization method has been supported by findings from both modeling [*Henderson et al.*, 1999] and sediment trap studies [*Scholten et al.*, 2001, 2005; *Yu et al.*, 2001].

[1]Auxiliary materials are available in the HTML. doi:10.1029/2008PA001693.

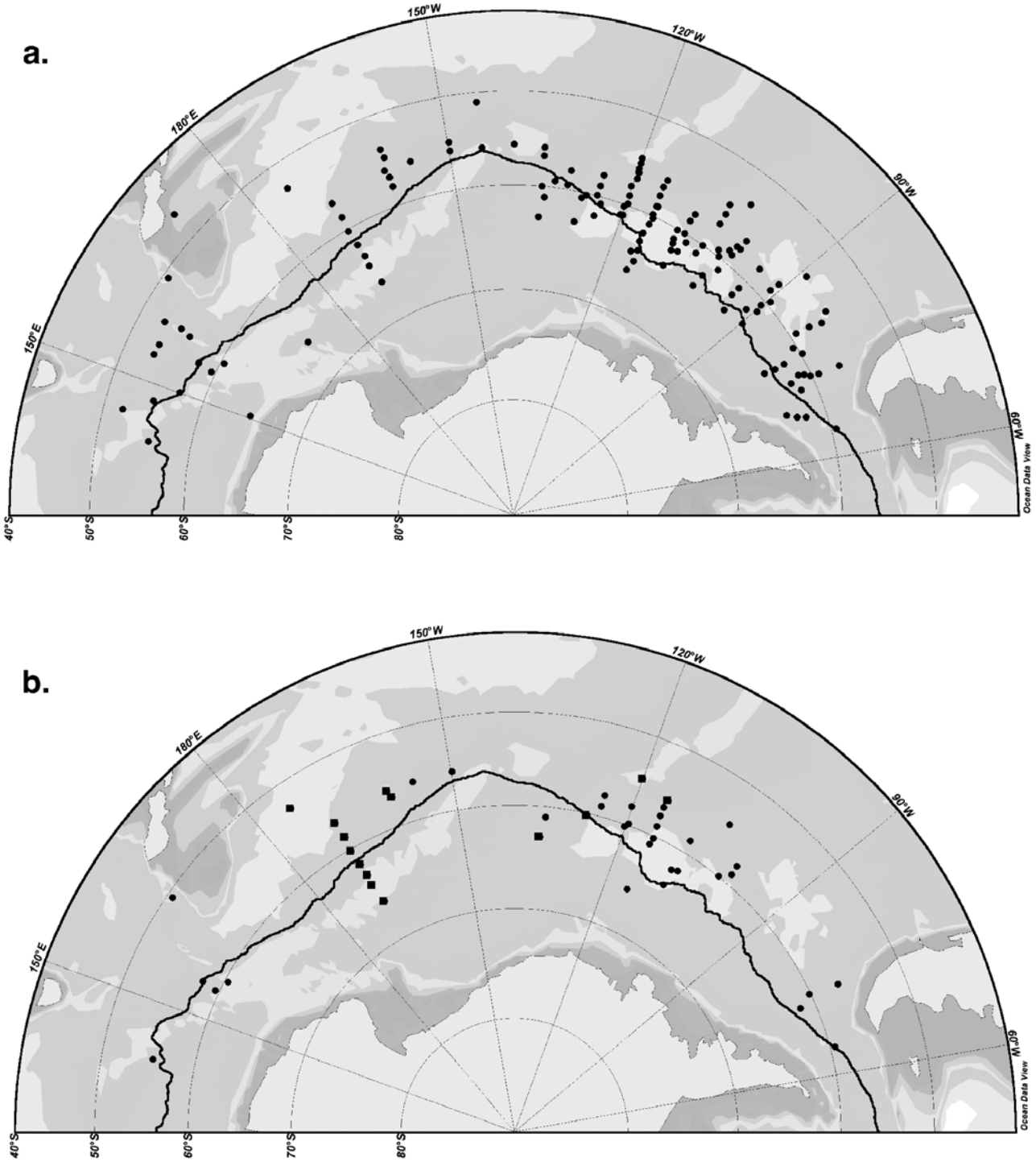

Figure 1. Locations of (a) all cores for which initial data were collected and (b) cores for which opal fluxes were derived. Solid circles represent new data from this study, while solid squares represent cores from *Chase et al.* [2003a]. The solid line represents the mean position of the Antarctic Polar Front as defined by *Orsi et al.* [1995].

[16] Setting the vertical flux of ^{230}Th equal to its known production rate, fluxes of preserved material can be calculated as: $F_i = \frac{C_i \times \beta \times z}{xs^{230}Th_0}$ where F_i is the flux of a sedimentary constituent of interest, C_i is the concentration of that constituent in bulk sediment, β*z is equal to the production rate of ^{230}Th in the water column (z is the depth of the water column (cm) and $\beta = 2.63*10^{-5}$ dpm cm^{-3} ka^{-1} (dpm, disintegrations per minute)), and $xs^{230}Th_0$ is equal to the decay-corrected concentration of Th in the sample (dpm g^{-1}) in excess of that supported by its parent, ^{234}U.

[17] Like ^{230}Th, ^{231}Pa is produced by radioactive decay of dissolved uranium (^{235}U), and is also removed from seawater by scavenging to particles. Protactinium has a longer residence time than thorium [*Anderson et al.*, 1983a, 1983b], so it can be transported over greater distances before being removed. Therefore, Pa tends to be removed in areas of higher scavenging, or areas with higher particle flux [*Lao et al.*, 1992, 1993; *Taguchi et al.*, 1989], and the ^{231}Pa/^{230}Th ratio (also decay corrected, and in excess of that supported by the respective parent isotopes) on particles and in sediments tends to increase with increasing particle flux. Protactinium is also preferentially scavenged by opal over other particle compositions [*Anderson et al.*, 1983a], and the opal/$CaCO_3$ ratio of particulate matter primarily dictates sedimentary ^{231}Pa/^{230}Th ratios in open-ocean regions with low fluxes of particulate lithogenic material, with total particle flux being a secondary contributor [*Chase et al.*, 2002, 2003b; *Walter et al.*, 1997]. As such, sedimentary ^{231}Pa/^{230}Th ratios and their deviation from the ^{231}Pa/^{230}Th production ratio of 0.093 add information about past changes in diatom productivity and, to some extent, dissolution. Since ^{231}Pa/^{230}Th ratios and opal fluxes are expected to vary somewhat in concert, deviations from this pattern could be interpreted as periods when opal was buried, incorporating high ^{231}Pa/^{230}Th ratios in the sediment, and later dissolved, leaving behind the ^{231}Pa/^{230}Th. This method is most useful in areas of low lithogenic flux [*Bradtmiller et al.*, 2006, 2007], and therefore must be applied with particular caution to SO samples of glacial age, which are known to have high lithogenic content and/or highly variable lithogenic fluxes.

5. Results

5.1. Core Composition

[18] Core composition data used to constrain age models are presented in Figures 2 for 28 of the 31 cores for which opal fluxes were derived. Cores V17-88TW, V17-90 and V18-73TW are not presented since they contain only two data points each. Within Figure 2 cores are placed in alphanumeric sequence. The full data set can be found at ftp://ftp.ncdc.noaa.gov/pub/data/paleo/contributions_by_author/bradtmiller2009/. Detailed descriptions of three cores, including illustrations of how those data were used to construct age models, can be found in the online auxiliary material.

5.2. Opal Fluxes, Lithogenic Fluxes, and ^{231}Pa/^{230}Th Ratios

[19] This section highlights several specific features of the new data from this study. Later, we will combine our results with those of *Chase et al.* [2003a] in order to produce a synthesis of glacial-Holocene changes in opal flux in the Pacific sector of the SO.

[20] Downcore records of opal flux, lithogenic flux and ^{231}Pa/^{230}Th ratio plotted against model age for each core can be seen in Figures 3, where cores are arranged in alphanumeric sequence. Cores V17-88TW, V17-90 and V18-73TW are again omitted. All cores south of the APF show greater Holocene than glacial opal flux (cores south of the APF, from north to south, are: E15-28, V18-93, E19-6, E19-7, RC8-71, E23-14, E36-36, E17-7, E27-23, E11-12). For example, E11-12 (65.87°S, 115.083°W, 4718 m, 3.67°S of the APF) shows fluxes of approximately 0.15 g cm^{-2} ka^{-1} during the LGP, as compared to fluxes twice that during the Holocene. Core RC8-71 (58.05°S, 155.733°E, 3224 m, 0.87°S of the APF) shows a similar pattern, with a glacial opal flux of 0.08 g cm^{-2} ka^{-1} compared to Holocene values between 0.45 and 0.28 g cm^{-2} ka^{-1}. Some cores such as V18-93 (from a site within the Drake Passage; 59.483°S, 64.783°W, 3834 m, 0.173°S of the APF) show a less discernable change, as LGP fluxes are only slightly less than Holocene fluxes, and both range from 0.06 to 0.09 g cm^{-2} ka^{-1}. The relatively small changes here may reflect unique constraints within the Drake Passage that limit glacial-interglacial changes in sea ice, circulation and, consequently, opal flux. While we can only speculate about the cause, it is interesting to note that the core from the Drake Passage has among the lowest opal fluxes and highest $CaCO_3$ fluxes of cores used in this study from sites on or south of the APF.

[21] North of the APF, ten of fifteen cores show greater glacial than Holocene opal fluxes (these cores, from north to south, are: V16-121, E11-3, E20-13, E11-4, E15-5, E15-12, E14-17, E15-4, E25-16, E15-6). This can be seen clearly in core V16-121 (50.667°S, 164.38°E, 3614 m, 9.413°N of the APF), as Holocene fluxes range from 0.064 to 0.147 g cm^{-2} ka^{-1}, while LGP fluxes range from 0.163 to 0.240 g cm^{-2} ka^{-1}. Other good examples include E11-3 (56.903°S, 115.243°W, 4023 m, 5.287°N of the APF; Holocene fluxes: 0.098–0.144 g cm^{-2} ka^{-1}; LGP: 0.247–0.300 g cm^{-2} ka^{-1}) and E15-5 (58.017°S, 99.983°W, 4307 m, 3.293°N of the APF; Holocene fluxes: 0.079–0.137 g cm^{-2} ka^{-1}; LGP: 0.327–0.417 g cm^{-2} ka^{-1}). A few cores show smaller LGP-Holocene changes, such as E15-4 (59.017°S, 99.758°W, 4910 m, 2.293°N of the APF; Holocene fluxes: 0.118–0.151 g cm^{-2} ka^{-1}; LGP: 0.167–0.197 g cm^{-2} ka^{-1}). The five remaining cores north of the APF show the opposite pattern, with Holocene fluxes exceeding LGP values (from north to south: E23-18, E23-17, E11-7, E21-20, V16-115). The largest LGP-Holocene difference is seen in E23-17 (60.217°S, 114.633°W, 5026 m, 1.98°N of the APF), where Holocene fluxes range from 0.611 to 0.700 g cm^{-2} ka^{-1}, as compared to LGP values between 0.230 and 0.329 g cm^{-2} ka^{-1}. Core E23-18 (58.983°S, 115.00°W, 5272 m, 3.22°N of the APF) shows the smallest difference, as the range of Holocene fluxes (0.548–0.554 g cm^{-2} ka^{-1}) falls within the variability of LGP fluxes (0.417–0.643 g cm^{-2} ka^{-1}).

[22] Figure 4 shows the difference between averaged LGP and averaged Holocene fluxes for each core, including data from *Chase et al.* [2003a], plotted as a function of distance from the APF. The average Holocene flux for a given core includes all samples between 0 and 10 ka, while the average LGP flux includes samples between 18 and 28 ka, as defined by our age models. It should be noted that some cores do not contain both LGP and Holocene data; these cores are omitted from Figure 4, but are included when plotting averaged LGP or Holocene data separately (see Figures 5 and 6). South of the APF, LGP-Holocene differences range from −1.71 to 0 g cm^{-2} ka^{-1}. North of the APF, differences range from −0.43 to 0.30 g cm^{-2} ka^{-1}.

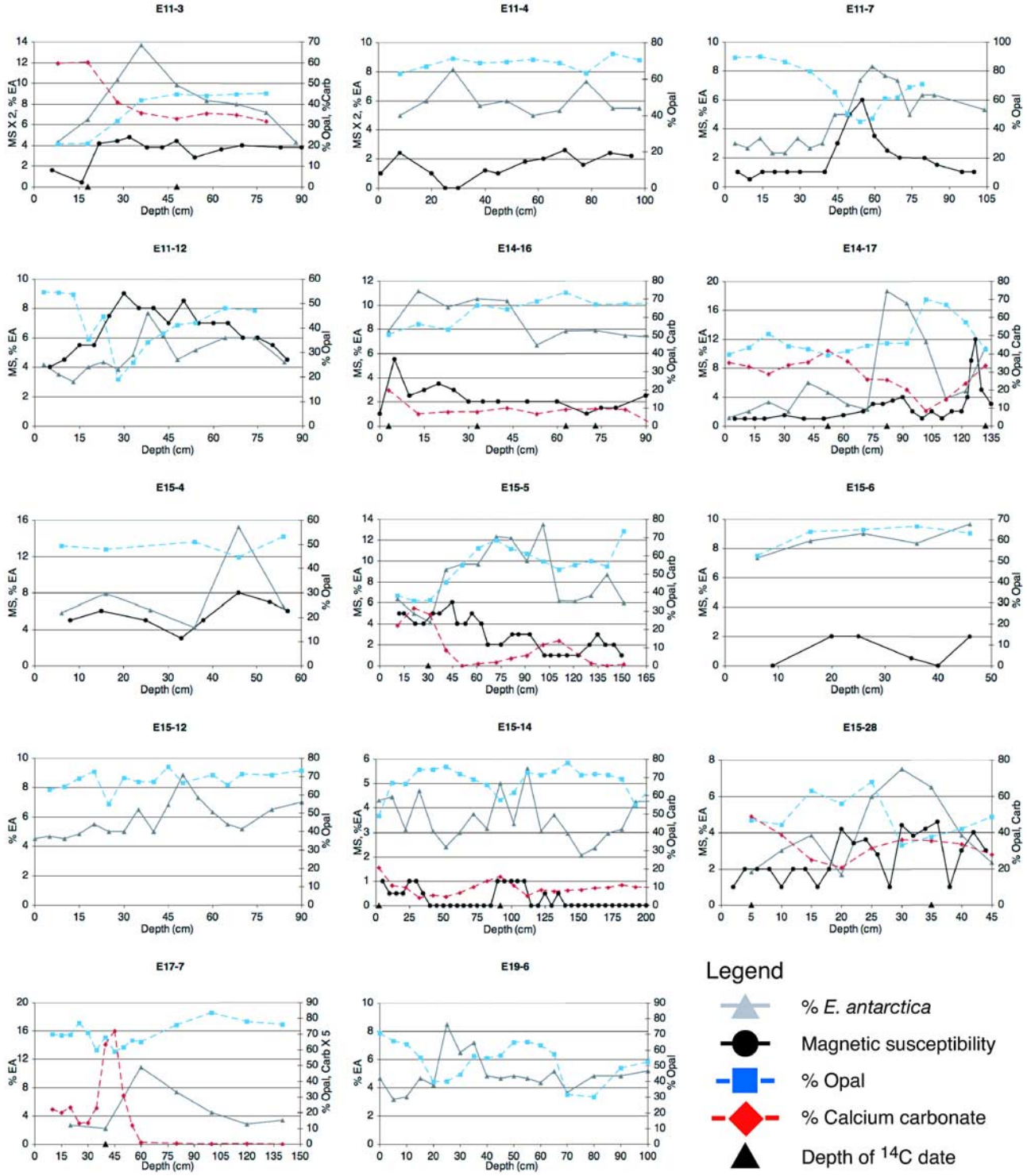

Figure 2. Sedimentary composition data used to constrain the age model for each core. All data are plotted versus depth within the core. Cores are arranged alphanumerically by name. The legend appears at the bottom. Locations, water depths, and positions relative to the APF are presented in Table 1.

The data form a general trend from the upper left hand quadrant (representing cores north of the APF for which LGP fluxes exceed Holocene fluxes) passing through and below the origin (i.e., cores at the APF with no glacial-Holocene difference in opal flux) into the lower right hand quadrant (representing cores south of the APF for which Holocene fluxes exceed those during the LGP).

[23] The difference between LGP and Holocene opal fluxes can also be seen in their spatial patterns (Figure 5). Maximum opal fluxes are seen near, or south of, the APF

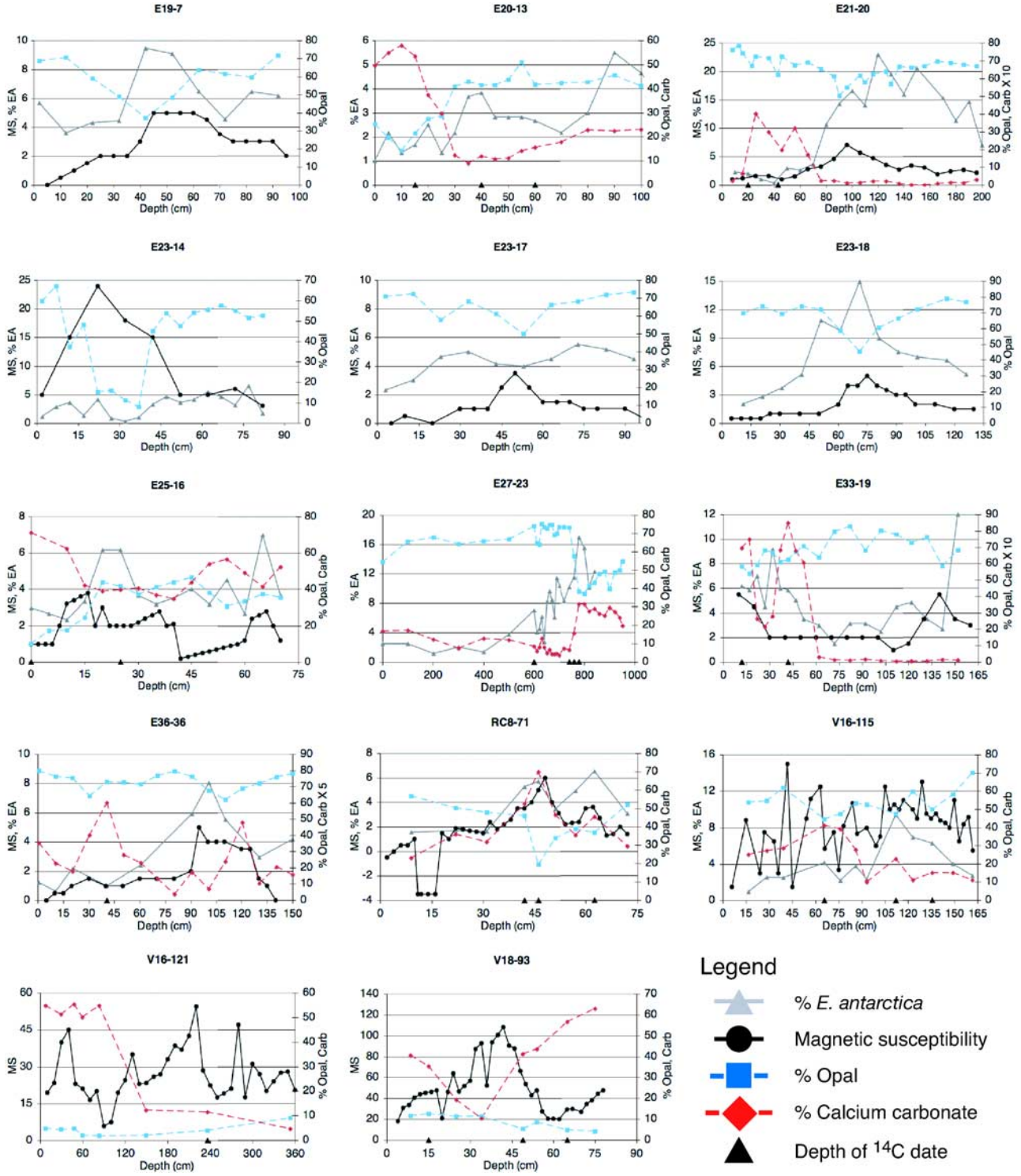

Figure 2. (continued)

during the Holocene (Figure 5b) but north of the APF during the LGP (Figure 5c). Furthermore, Holocene opal fluxes in the western part of the basin are generally greater than in the east (Figure 5b). It is noteworthy that this zonal pattern in Holocene ^{230}Th-normalized opal flux is consistent with east–west gradients in phytoplankton biomass inferred from satellite ocean color data (Figure 5a) (G. C. Feldman, SeaWiFS biosphere globes, 2008, available at http://oceancolor.gsfc.nasa.gov/cgi/biosphere_globes.pl, NASA/GSFC).

[24] Fluxes of lithogenic material during the Holocene exhibit relatively little small-scale spatial variability, varying between roughly 0.1 and 0.2 g cm^{-2} ka^{-1} throughout most of the region (Figure 6a). Consequently, on occasions where we found an apparent lithogenic flux much larger

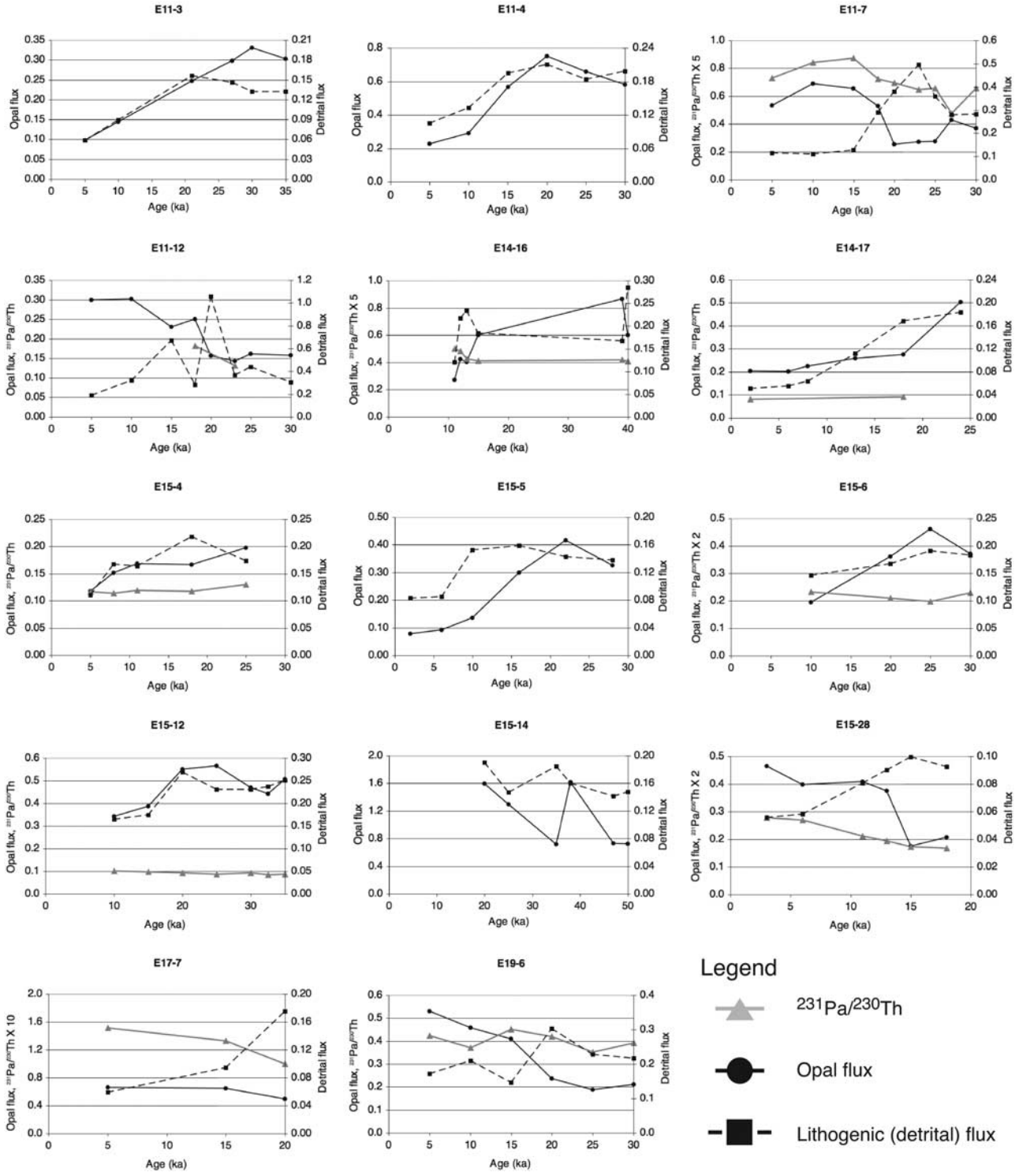

Figure 3. Opal and lithogenic (detrital) fluxes and $^{231}Pa/^{230}Th$ ratios in each core. Results are plotted against age using age models developed as described in the online auxiliary material. Cores are arranged alphanumerically by name. The legend appears at the bottom.

than this in core top sediments bearing interglacial characteristics, the anomalously high lithogenic flux provided a clue that the last glacial cycle was missing (see online auxiliary material). Although Holocene fluxes are relatively uniform, an increase from west to east is detectable (Figure 6a), indicating a supply of lithogenic material to the central portion of the Pacific sector of the Southern Ocean, presumably carried by icebergs. Lithogenic fluxes during the LGP are uniformly greater than during the Holocene, but small-scale spatial variability remains modest. The most

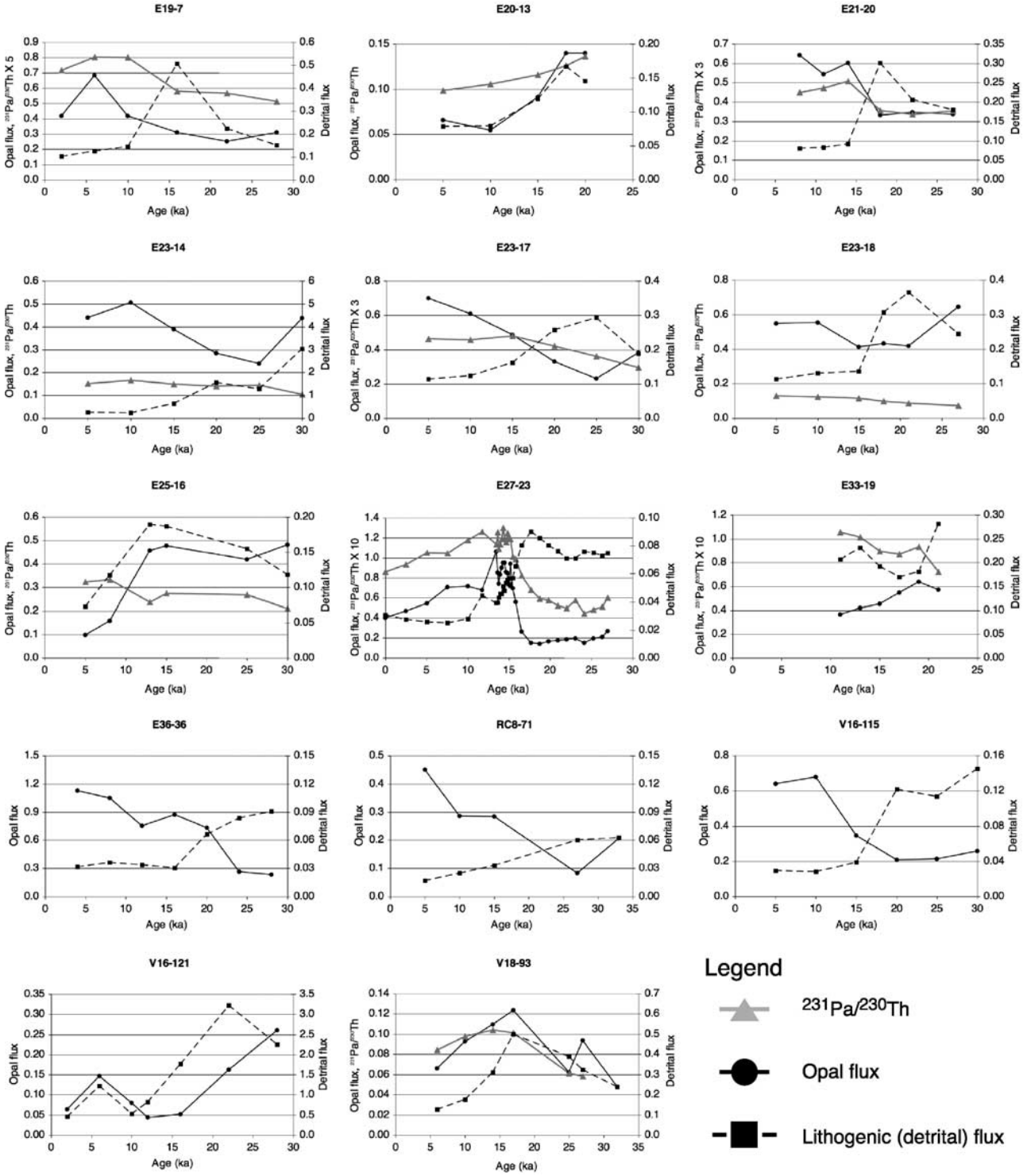

Figure 3. (continued)

significant increase occurs in the eastern part of the basin, near the APF, where fluxes are much larger than average (Figure 6b). Apparently, the source of lithogenic material into the central part of the Pacific sector evident in Holocene results (see above) was accentuated during the LGP.

[25] Because ^{231}Pa is preferentially scavenged by opal, the ^{231}Pa/^{230}Th ratio of sediments reflects their opal content to some extent (see section 3). Therefore, we expect downcore covariance of opal flux and the ^{231}Pa/^{230}Th ratio if opal dissolution has remained approximately constant through time. The data show several examples of opal and ^{231}Pa/^{230}Th covariance within a core, including E21-20 (60.25°S, 120.17°W, 4701 m, 0.11°N of the APF), in which opal flux and the ^{231}Pa/^{230}Th ratio show steady values

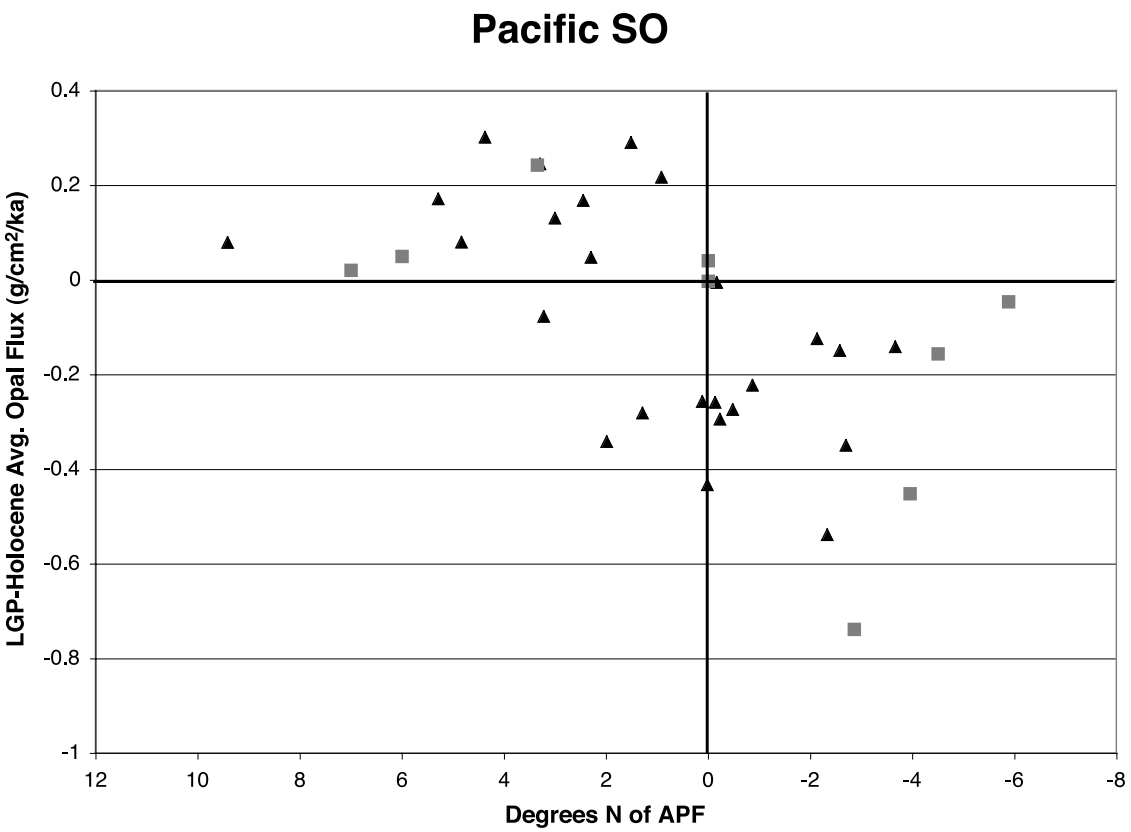

Figure 4. The difference between average LGP (18–28 ka according to our age models) and average Holocene (0–10 ka according to our age models; see the online auxiliary material) opal flux for each core, plotted as a function of distance from the APF as defined by *Orsi et al.* [1995].

throughout the LGP (^{231}Pa/^{230}Th: 0.112–0.119; see Figure 3), increase between 18 and 15 ka (^{231}Pa/^{230}Th: 0.169), and remain fairly constant during the Holocene (^{231}Pa/^{230}Th: 0.150–0.157). Core E27-23 (59.62°S, 155.24°E, 3182 m, 2.70°S of the APF) also shows a strong relationship between opal flux and ^{231}Pa/^{230}Th where both proxies are at fairly constant values during the LGP (^{231}Pa/^{230}Th: 0.045–0.060), increase sharply at 15 ka (^{231}Pa/^{230}Th: 0.119), and decline steadily throughout the Holocene (^{231}Pa/^{230}Th: 0.126–0.086). Some cores show almost no covariance between opal and the ^{231}Pa/^{230}Th ratio, however, including E14-16, E15-6, E15-12, E25-16 and E33-19. Section 6.1 explores possible explanations for the lack of correlation between opal and the ^{231}Pa/^{230}Th ratio in these cores.

6. Discussion

6.1. Preservation Versus Production

[26] Calculating and interpreting opal fluxes is hardly ever straightforward. The amount of opal buried at a given site depends on diatom productivity in the surface ocean, opal dissolution in the water column, and the lateral transport of sediment along the seafloor by bottom currents, all of which potentially change through time. Earlier work in the modern Southern Ocean suggested that the SO is an area of anomalously high opal preservation [e.g., *Nelson et al.*, 1995] in order to explain the large amount of opal buried beneath a seemingly low productivity region, the so-called "opal paradox." However, this discrepancy has largely been reconciled by downward revisions of opal fluxes through the use of ^{230}Th normalization, and through upward revisions in the estimated surface production rate [*Frank et al.*, 2000; *Geibert et al.*, 2005; *Nelson et al.*, 2002; *Pondaven et al.*, 2000; *Tréguer et al.*, 1995]. These data have shown that the range of opal preservation in the SO (1.2–5.5%) [*Nelson et al.*, 2002] is within a factor of two of the global mean (2.5 ± 0.9%) [*Tréguer et al.*, 1995].

[27] Our study seeks to use the opal burial rate as a proxy for diatom productivity. Because such a large percentage of opal produced at the surface is eventually dissolved, it is important to verify that spatial patterns of opal burial in SO surface sediment reflect spatial patterns of diatom productivity in the surface ocean. To do this, we compare calculated ^{230}Th-normalized Holocene opal fluxes to satellite estimates of chlorophyll concentration in our sample area (Figure 5). This comparison shows that our Holocene data captures the high-productivity region in the central portion of the Pacific sector of the SO (~115°W–180°), as well as the low-productivity region in the eastern part of the basin (~60°W–115°W). Although diatoms are not the only taxa contributing to the ocean color signal obtained from SeaWiFS, they are a dominant taxa in the Southern Ocean, and the general agreement lends confidence that we are assessing correctly both spatial and temporal patterns of diatom productivity by evaluating ^{230}Th-normalized opal fluxes.

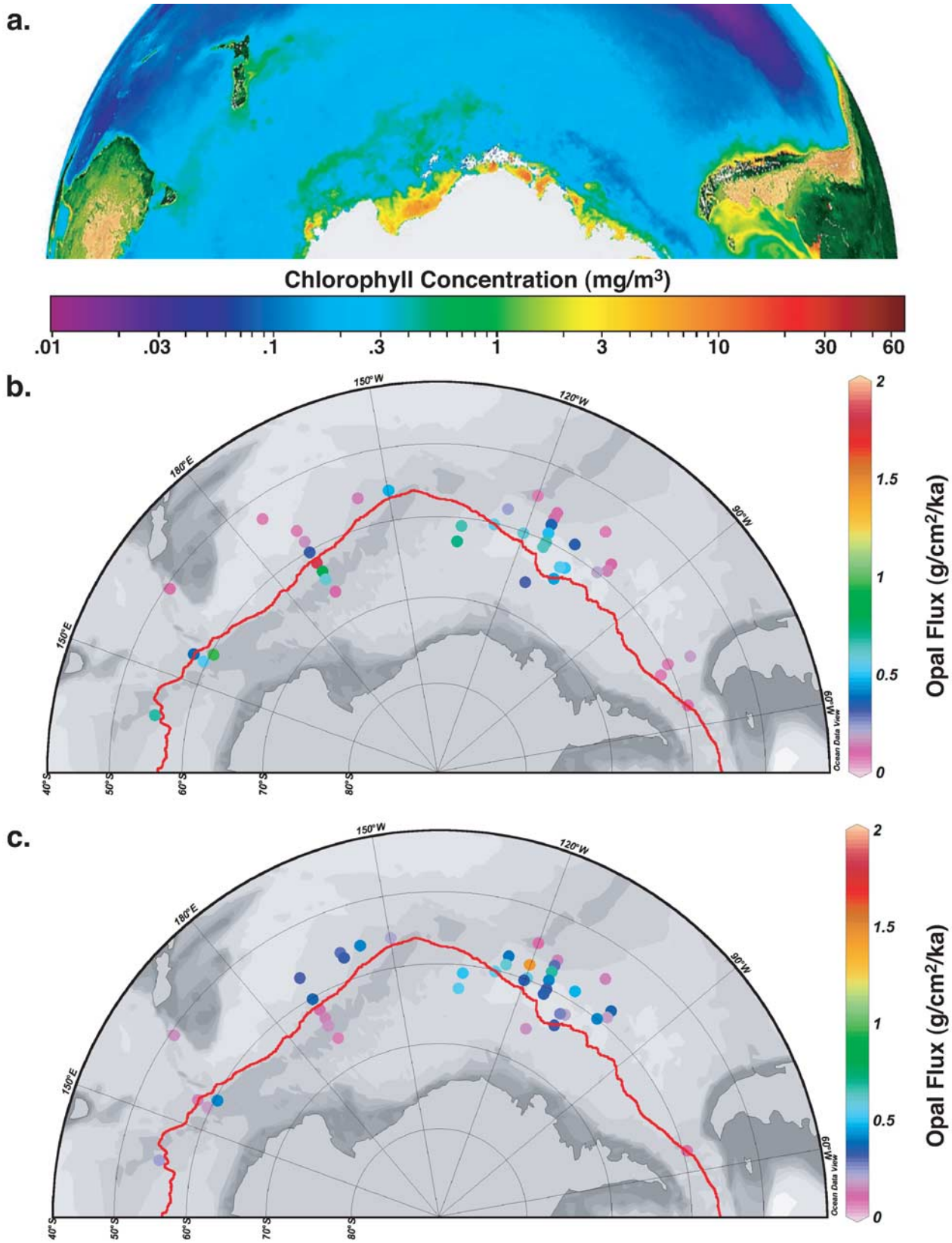

Figure 5. Maps of (a) Pacific SO austral summer chlorophyll concentration (G. C. Feldman, SeaWiFS biosphere globes, 2008, available at http://oceancolor.gsfc.nasa.gov/cgi/biosphere_globes.pl, NASA/GSFC), (b) Holocene opal fluxes, and (c) LGP opal fluxes. The red line denotes the APF as defined by *Orsi et al.* [1995]. Opal fluxes include those from Figure 3 and results from *Chase et al.* [2003a].

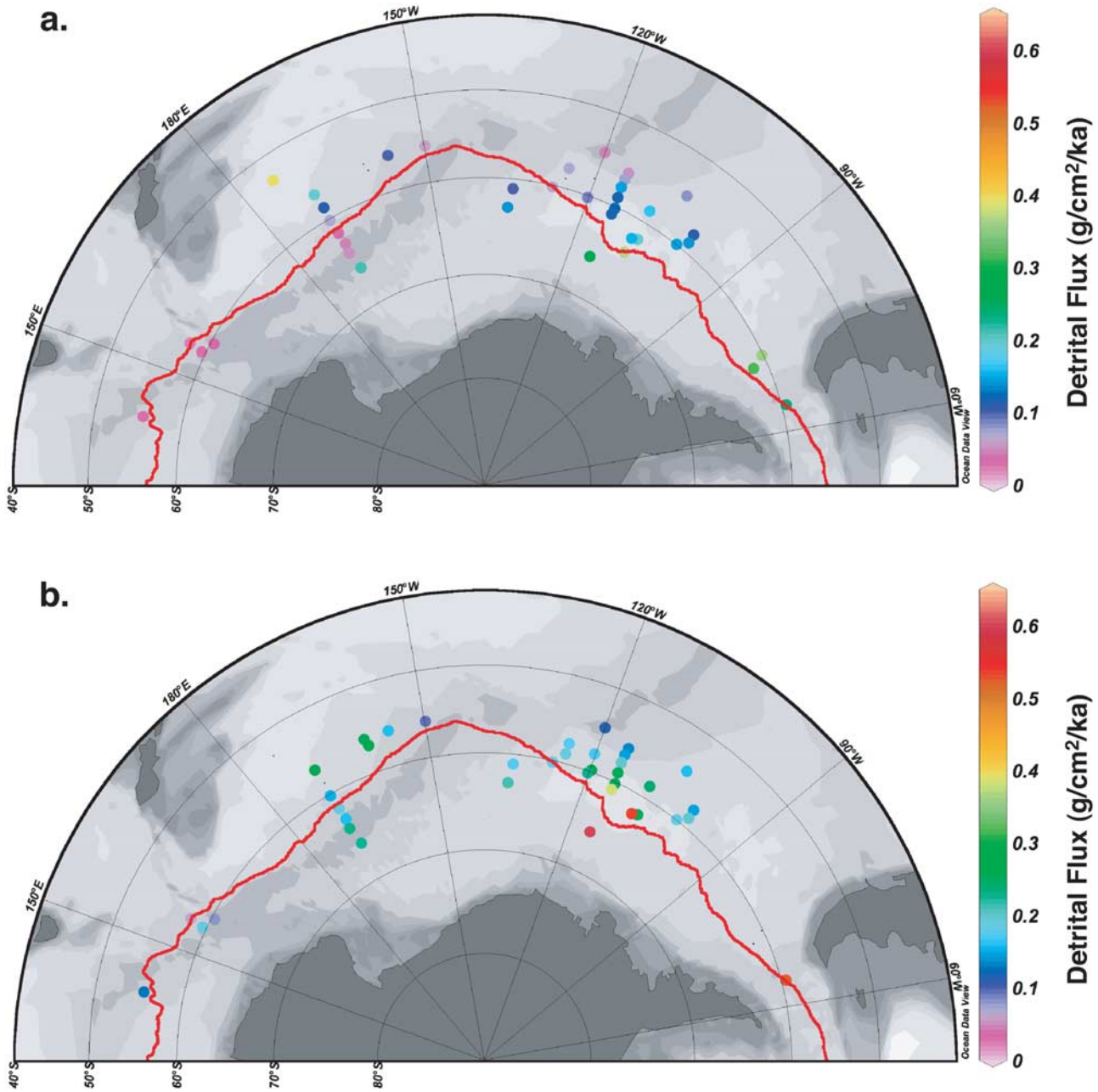

Figure 6. Maps of (a) Holocene lithogenic (detrital) fluxes and (b) LGP lithogenic fluxes. Note that the maps do not include cores V16-121 (50.667°S, 164.38°E) (Holocene and LGP) and V17-88 (57.033°S, 74.483°W) (Holocene), which are near land and therefore have high detrital fluxes, or core E23-14 (63.817°S, 108.85°W) which has a flux during the LGP that is off scale. The red line denotes the APF as defined by *Orsi et al.* [1995]. Lithogenic fluxes include those from Figure 3 and results from *Chase et al.* [2003a].

[28] Because we do not have chlorophyll images of the glacial ocean, we must verify to the best of our ability that dissolution did not change dramatically in the glacial-interglacial interval, and assume that the relationship between spatial patterns of surface productivity and opal flux to the sediment holds true over this timescale. The $^{231}Pa/^{230}Th$ ratio has been used to this effect in other studies (see section 4), because ^{231}Pa adsorbs preferentially to opal, while ^{230}Th adsorbs preferentially to carbonate and lithogenic material. Many of the downcore records presented here show very good correlation between opal flux and the $^{231}Pa/^{230}Th$ ratio (e.g., E17-7, E19-7, E21-20, E27-23 and V18-93), suggesting that the records are minimally affected by changes in dissolution. Some records are uncorrelated with respect to these two variables (e.g., E14-16, E15-6, E15-12, E25-16 and E33-19), however it should be noted that these five cores are located north of the APF. In this region, high lithogenic fluxes during the LGP may have

exerted a competing effect on the $^{231}Pa/^{230}Th$ ratio. That is, while opal fluxes were higher during the LGP, leading to increased scavenging of ^{231}Pa, lithogenic fluxes were also greater, leading to increased scavenging of ^{230}Th. South of the APF, these two factors would have worked in concert, as opal fluxes were decreased and lithogenic fluxes increased during the glacial period relative to the Holocene. We must therefore apply the $^{231}Pa/^{230}Th$ ratio with caution as an opal dissolution indicator, particularly north of the APF. With this caveat, $^{231}Pa/^{230}Th$ ratios south of the APF suggest that opal fluxes reflect changes in diatom productivity rather than changes in preservation, so we infer that the same is true north of the APF as well.

6.2. Testing the SALH

[29] The SALH as originally presented [*Brzezinski et al.*, 2002; *Matsumoto et al.*, 2002a] invoked greater export of Si from the Southern Ocean to the tropics during glacial periods, compared to interglacials, to account for the lower glacial CO_2 levels in the atmosphere (section 1). If true, then this implies a reduction in Si utilization in the Southern Ocean relative to Si supply by upwelling. That is, it is the difference between supply and utilization, rather than the absolute value of either, that regulates Si export to the tropics. Consequently, in order to test the SALH, both supply and utilization must be constrained. Past changes in Si utilization can be indirectly estimated by measuring fluxes of opal preserved and buried in sediments, as we present here. However, there is no measurable proxy for Si supply, so an indirect line of reasoning must be applied.

[30] Some authors have argued for reduced upwelling in the glacial Southern Ocean as the primary cause of lower CO_2 levels in the glacial atmosphere [*Francois et al.*, 1997; *Sigman and Boyle*, 2000]. Were that the case, then one would expect the supply of Si by upwelling to have been lower during glacial periods, as well. Consequently, since virtually all of the Si supplied by upwelling to the region around the APF is consumed by diatoms [*Pondaven et al.*, 2000; *Sigmon et al.*, 2002; *Smith et al.*, 2000], one would expect the average opal flux integrated across the Southern Ocean to have been lower as well. Contrary to this expectation, as noted above, the average opal flux in the Atlantic and Indian sectors of the Southern Ocean during the LGM was indistinguishable from that of the Holocene [*Dezileau et al.*, 2003; *Francois et al.*, 1997; *Frank et al.*, 2000; *Kumar et al.*, 1995]. The similarity between average opal fluxes in glacial and Holocene sediments has been used to argue that wind driven upwelling in the Southern Ocean may not actually have been less during glacial periods than during interglacials [*Anderson et al.*, 2002]. Whether or not this argument can be applied to the volume of water upwelled, the supply of Si by upwelling during the LGP cannot have been much less than during the Holocene because opal fluxes must have been lower if that were the case, given that nearly all of the upwelled Si is consumed today.

[31] If we accept that the supply of Si by upwelling during the LGP was not significantly less than during the Holocene in the Atlantic and Indian sectors, as required by the similar average opal fluxes during the LGM and Holocene, then we reason that the supply of Si by upwelling in the Pacific sector was likely as large during the LGP as during the Holocene as well. This reasoning is based on the fact that upwelling and nutrient supply are driven by the Westerlies, which are circumpolar in extent. Therefore, if supply of Si by upwelling in the Atlantic and Indian sectors could have been no less during the LGP than during the Holocene, then the same conditions are likely to have existed in the Pacific sector as well. Consequently a glacial reduction in opal flux can be interpreted to reflect a glacial reduction in Si utilization in the Pacific sector of the SO, leaving more Si to be exported to the tropics.

[32] In order to compare glacial and Holocene opal fluxes, we derived average values for the Pacific sector of the SO for both periods. Because our sample sites (including those of *Chase et al.* [2003a]) include a larger number of cores north of the APF (n = 28) than cores on or south of the APF (n = 17), we first constructed LGP and Holocene averaged fluxes of all cores within each of three latitude zones: greater than 1° north of the APF (n = 24), within 1° of the APF (n = 11), and greater than 1° south of the APF (n = 10). These fluxes were calculated by averaging the average LGP and Holocene fluxes from each core (see Figures 4 and 5). We subsequently compiled a weighted average of the results from all three regions in order to estimate average LGP and Holocene opal fluxes for the Pacific SO (Table 3). Results were weighted by degrees latitude spanned by each region (5 for the regions north and south of the APF, and 2 for the region within a degree of the APF). The combined data set suggests a 29% decrease in Pacific sector opal burial during the last glacial period (0.319 g cm^{-2} ka^{-1}) as compared to the Holocene (0.447 g cm^{-2} ka^{-1}). These data capture the previously observed northward shift in opal flux during the LGP, and suggest that the increase in opal flux north of the APF during the LGP was not great enough to offset decreased opal burial to the south, resulting in less total opal burial during the LGP across the entire region.

[33] In order to estimate the uncertainties associated with core-to-core variability in our data set, we performed a resampling of the data (LGP-Holocene opal flux) using the null hypothesis that there is no difference in total opal burial between the Holocene and the LGP. We performed two experiments; in the first, we selected one core from the group >1° north of the APF, one core within 1° north/south of the APF, and one core >1° south of the APF, and used data from these three cores to calculate the weighted average LGP-Holocene difference in opal flux. We then repeated the calculation using every possible combination of cores (n = 2640). In the second experiment, we selected random LGP and Holocene data points from each region and performed the same calculation, repeated 10,000 times. Figure 7 shows histograms (Figures 7a and 7b) and probability distribution functions (PDFs) (Figure 7c) of the experimental results; note that the majority of the data fall in the negative (LGP < Holocene) portion of the graph. The exact likelihood of obtaining a negative LGP-Holocene average opal flux can be derived by taking the value of the PDF at the 0 g cm^{-2} ka^{-1} mark (exp. 1: 77.5%, exp. 2: 67.7%). The results of these two experiments show that while we cannot rule out the null hypothesis that Holocene opal fluxes were no different than those of the LGP, it is very likely that

Table 3. Average Holocene and LGP Opal Fluxes for the Pacific SO and Estimated Total Opal Burial Rates[a]

	Holocene[b]		LGP[c]	
	Flux ($g\ cm^{-2}\ ka^{-1}$)	Standard Error ($g\ cm^{-2}\ ka^{-1}$)	Flux ($g\ cm^{-2}\ ka^{-1}$)	Standard Error ($g\ cm^{-2}\ ka^{-1}$)
>1°N of APF	0.203	0.042	0.385	0.068
±1° of APF	0.429	0.056	0.306	0.048
>1°S of APF	0.699	0.149	0.258	0.054
All regions (weighted)	0.447	0.104	0.319	0.073
Chase et al. [2003a] data only	0.452	-	0.256	-
	Holocene[b]		LGP[c]	
	Opal Burial ($Gt\ ka^{-1}$)	Standard Error ($Gt\ ka^{-1}$)	Opal Burial ($Gt\ ka^{-1}$)	Standard Error ($Gt\ ka^{-1}$)
Pacific SO	53.0	12.3	37.8	8.6

[a]See sections 6.2 (fluxes) and 6.4.1 (burial rates) for descriptions of calculation methods.
[b]Holocene is from 0 to 10 ka.
[c]LGP is from 18 to 28 ka.

Holocene opal fluxes in fact exceeded LGP opal fluxes. These experiments estimate the likelihood of obtaining a different result using a subsample of our available data, and cannot (by definition) estimate the likelihood of obtaining a different result had we originally sampled different cores. However, we suggest that given the internal consistency of our data as well as its consistency with previously published results, this represents a reasonable estimate of uncertainty. Therefore, all further discussion and analysis in this manuscript will reflect the assumption that our data are robust, and that there was in fact less opal buried in the Pacific Southern Ocean during the glacial period than the Holocene.

[34] Results from this study seem to support the earlier view [*Chase et al.*, 2003a] that opal burial in the Pacific sector of the Southern Ocean was less during the LGP than during the Holocene. Combined with the reasoning described above that supply of Si by upwelling would have been no less during the LGP than during the Holocene,

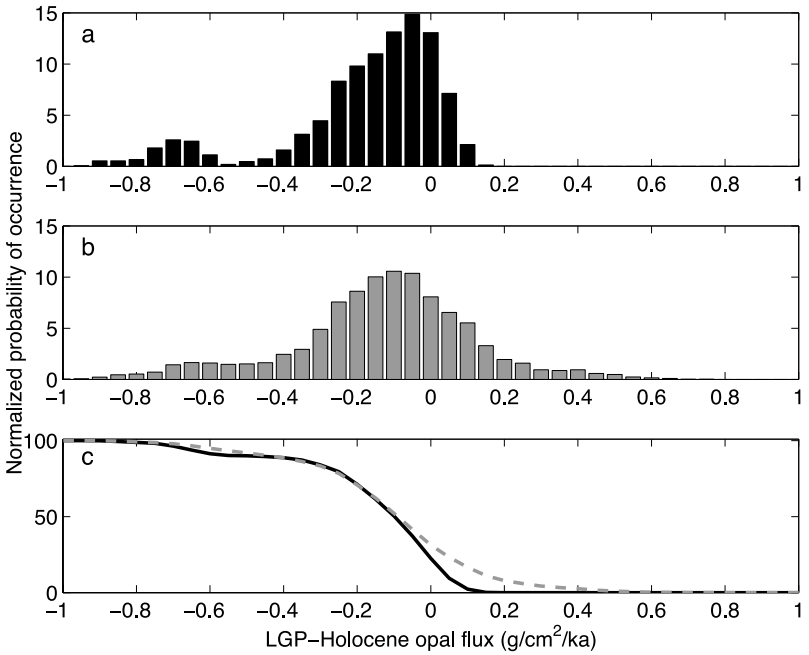

Figure 7. Results of two data resampling experiments using the null hypothesis: LGP opal burial equals Holocene opal burial. The first experiment randomly selected three cores, one each from north of, within, and south of the APF, and used data from these cores to construct weighted average LGP and Holocene opal fluxes. This was repeated with all possible core combinations. The second experiment randomly selected Holocene and LGP data points (i.e., not necessarily from the same core) within each geographic area to make the same calculation, repeated 10,000 times. Here we show histograms of results from experiments (a) 1 and (b) 2 as probabilities normalized to 100. (c) The resulting probability distribution functions are color coded to match the histograms.

these findings support, or at least allow for, the premise of the SALH that the export of dissolved Si from the Southern Ocean to the tropics was greater during the LGP than during the Holocene. In presenting these conclusions we recognize the two significant sources of uncertainty: (1) the indirect reasoning required to constrain the supply of Si by upwelling during the LGP, and (2) the large statistical uncertainty in the average LGP and Holocene opal fluxes (Table 3) associated with the core to core variability in our results. Nevertheless, the growing evidence presented here supports one premise of the SALH, thereby encouraging further work to test the hypothesis. The following sections will place these findings in the context of other data from the Southern and tropical oceans in an attempt to synthesize the evidence in support of and contrary to the SALH, and to identify areas for future research.

6.3. Comparison With Silicon Isotope Data

[35] Silicon isotope ratios (notated δ^{30}Si) have been used extensively in attempts to test the SALH, as they can be used as proxies for changes in surface Si utilization efficiency [*De La Rocha et al.*, 1997, 1998]. The proxy works on the principle that diatoms discriminate against silicic acid containing the heavier isotope (^{30}Si) in favor of ^{28}Si. As diatoms consume the lighter isotope preferentially (forming opal with low δ^{30}Si), the residual pool of dissolved Si becomes isotopically heavier, or increased in δ^{30}Si. Subsequent diatom productivity will therefore result in opal with more positive δ^{30}Si values. In other words, the greater the fraction of available Si consumed, the greater the δ^{30}Si of diatom opal averaged over the growing season and preserved in sediments.

[36] Both north and south of the APF in the Atlantic and Indian sectors of the SO, δ^{30}Si values of sedimentary opal were lower during the glacial period than the Holocene [*Beucher et al.*, 2007; *Brzezinski et al.*, 2002; *De La Rocha et al.*, 1998]. This has been interpreted as evidence of reduced Si utilization during the glacial period, because of the relief of iron stress on SO diatoms and the resulting decrease in their Si:N uptake ratios [*Franck et al.*, 2000]. Coupled with evidence for decreased glacial opal burial in the Pacific Southern Ocean [*Chase et al.*, 2003a], these data formed the basis of the SALH prediction that excess Si escaped the glacial SO.

[37] However, there is another viable explanation for the δ^{30}Si results that does not require lower overall Si utilization in the SO during the LGP. If any factor (e.g., increased sea ice extent) limited diatom productivity south of the APF during the LGP, assuming that the supply of upwelled Si and its isotopic composition remained constant, then diatoms would have consumed a smaller fraction of the Si pool than today, lowering the δ^{30}Si of opal buried in sediment, as observed. This scenario is also consistent with the observed decrease in opal burial south of the APF during the LGP (this study and *Chase et al.* [2003a]).

[38] Under this scenario, the δ^{30}Si of the residual pool of dissolved Si in surface waters south of the APF would then have been lower than today, as well. If northward mixing of residual nutrients carried by Antarctic Surface Waters represents the principal source of dissolved Si north of the APF, as it does for nitrate [*Sigman et al.*, 1999], then the δ^{30}Si of opal produced north of the APF would be sensitive to changes in the δ^{30}Si of the residual Si south of the APF. In other words, if the source of dissolved Si to the region north of the APF was isotopically lighter during the LGP, then the δ^{30}Si of opal north of the APF could have been less than today, as observed in the sediments, even if all of the dissolved Si was consumed. Consequently, the δ^{30}Si of opal cannot be used as unequivocal evidence for lower overall Si utilization in the glacial Southern Ocean. This uncertainty necessitates the use of alternative strategies to test the SALH, such as the mass budget approach pursued here.

6.4. Global Synthesis

[39] In addition to the Southern Ocean, tests of the SALH have been conducted in the tropics, where excess Si is predicted to upwell if it escaped the Southern Ocean. This section seeks to interpret the results of this study within the context of previous work on the SALH, as well as other paleoceanographic studies in the tropics.

6.4.1. Opal Budget Comparisons

[40] Opal records from the equatorial oceans show mixed results with regard to the prediction of the SALH that opal burial in tropical upwelling regions should have been greater during the LGP than during the Holocene in the absence of major changes in ocean circulation. In the eastern equatorial Pacific Ocean, two studies found less opal flux during the last glacial period than during the Holocene [*Bradtmiller et al.*, 2006; *S. S. Kienast et al.*, 2006], in contrast to the predictions of the SALH. This is particularly significant because the eastern part of the basin is where the strongest upwelling of SO water occurs today [*Toggweiler et al.*, 1991], and where *Sarmiento et al.* [2004] predicted the strongest increase in glacial opal flux. In addition, *Bradtmiller et al.* [2006] found that opal flux across the equatorial Pacific Ocean (80°W–145°E, 5°N–5°S) was less during the last glacial period than the Holocene, implying that this change occurred over most of the basin, not only regionally. Using averaged Holocene and LGP fluxes applied over this area, *Bradtmiller et al.* [2006] estimated that Holocene opal burial in the equatorial Pacific occurred at a rate of approximately 10.9 Gt opal ka^{-1}, while LGP burial averaged 8.1 Gt opal ka^{-1}.

[41] Conversely, equatorial Atlantic opal data support the predictions of the SALH. Downcore records of opal mass accumulation rate [*Verardo and McIntyre*, 1994], diatom accumulation [*Abrantes*, 2000] and ^{230}Th-normalized opal flux [*Bradtmiller et al.*, 2007] all show increased values during the last glacial period as compared to the Holocene. This pattern is evident in both eastern and western cores [*Bradtmiller et al.*, 2007; *Verardo and McIntyre*, 1994]. *Bradtmiller et al.* [2007] applied average LGP and Holocene fluxes over the area 0°–40°W, 5°N–5°S, resulting in estimates of LGP (3.3 Gt opal ka^{-1}) and Holocene (1.5 Gt opal ka^{-1}) opal burial rates for the tropical Atlantic. The glacial-interglacial difference in the Atlantic (1.8 Gt opal ka^{-1}) is similar to that of the Pacific (2.8 Gt opal ka^{-1}), but of opposite sign. If only the easternmost 40° of the Pacific are considered (the region of highest productivity), then the

difference is 1.8 Gt opal ka^{-1}, equal in magnitude but opposite in sign to the Atlantic.

[42] In this study we found that average opal burial in the Pacific sector of the Southern Ocean was 29% lower during the LGP relative to the Holocene. To compare this with results from the tropics, we applied the calculated LGP and Holocene opal fluxes (Table 3) over an area of 1.2×10^7 km^2, representing 54°S–66°S (6° north and south of the average position of the APF), and 60°W–140°E (the zonal extent of cores used in this study). This yields Holocene and LGM burial rates of 53.0 and 37.8 Gt opal ka^{-1}, respectively (Table 3). The difference, 15.2 Gt opal ka^{-1}, is larger than the burial of opal in the equatorial Atlantic and Pacific oceans combined. We acknowledge the uncertainties inherent in using this method, and calculations of standard error of the mean are also included in Table 3. We also remind the reader that a statistical resampling of the data does not allow us to rule out the null hypothesis that there was no significant difference between Holocene and LGP opal fluxes (see section 6.2). However, taking at face value the primary result of this calculation (i.e., that Holocene opal burial exceeded that of the LGP), and given the high rates of modern opal burial and the extremely large area of opal accumulation in the Southern Ocean, even a somewhat smaller change in the average opal flux over this area would result in a net LGP Si deficit much larger in scale than the changes observed in the tropics.

[43] These data provide a new scale for comparison between the three areas of the ocean most likely to be involved in the SALH. We infer from our results that a great deal of unused Si escaped the glacial Southern Ocean through the Pacific sector, but the eventual destination of this Si remains a mystery. Less opal was buried in the glacial equatorial Pacific Ocean than today, effectively ruling it out as a possible sink. The equatorial Atlantic Ocean experienced a glacial increase in opal burial, but the scale of this change is an order of magnitude smaller than the projected export of dissolved Si from the Pacific sector of the SO. One possible destination for the Si exported from the Southern Ocean is enhanced opal burial along continental margins [*DeMaster*, 2002], which has the potential to alter the C_{org}:$CaCO_3$ ratio of sediment, and would be an interesting topic for further exploration. However, the relatively small magnitude of glacial-interglacial changes in equatorial opal burial, in addition to the fact that changes in the Atlantic and Pacific Oceans are opposite in sign and therefore negate each other in the global budget, suggests that their behavior over the last glacial cycle may have been influenced primarily by factors other than changes in Si export from the SO.

6.4.2. Changes in Equatorial Upwelling

[44] One interpretation of the observed changes in opal burial in equatorial sediments is that changes in equatorial diatom productivity were driven largely by changes in upwelling and had little or no connection to Si leakage from the Southern Ocean. In other words, glacial productivity of all phytoplankton taxa may have been greater in the equatorial Atlantic Ocean (and less in the equatorial Pacific Ocean) because of changes in upwelling and/or the depth of the nutricline on a regional scale. Data from the glacial equatorial Atlantic show evidence of increased rates of upwelling because of more vigorous glacial trade winds [*CLIMAP project members*, 1976; *M. Kienast et al.*, 2006], and *F. profunda* data suggest that the nutricline was shallower because of increased upwelling [*Henriksson*, 2000; *McIntyre and Molfino*, 1996; *Molfino and McIntyre*, 1990]. New Mg/Ca data suggest that sea surface temperatures across the entire basin were cooler during the LGM, which has also been interpreted as evidence of increased upwelling rates (J. Arbuszewski and P. B. DeMenocal, manuscript in preparation, 2009). The presence of a shallower nutricline due to increased upwelling would have increased the total nutrient supply and therefore overall productivity (not just productivity of diatoms) in the Atlantic, consistent with the observed glacial increase in opal burial. This possibility is supported by studies indicating that coccolithophorid productivity in the equatorial Atlantic also increased during the last glacial period [*Henriksson*, 2000].

[45] In contrast to the Atlantic, there is less consistency among interpretations of paleoproductivity in the equatorial Pacific Ocean. Fluxes of biogenic sediments [*Farrell et al.*, 1995; *Lyle*, 1988] and of barite [*Paytan et al.*, 1996] were interpreted to indicate greater productivity during the LGM compared to the Holocene. However, when biogenic fluxes are reassessed by normalizing to ^{230}Th to correct for sediment focusing, glacial fluxes are found to be less then or equal to those of the Holocene [*Bradtmiller et al.*, 2006; *S. S. Kienast et al.*, 2006; *Loubere et al.*, 2004; *Pichat et al.*, 2004]. Furthermore, independent evidence based on coccolithophorid communities [*Beaufort et al.*, 2001] and benthic foraminifera assemblages [*Loubere*, 2000] are consistent with the ^{230}Th-normalized fluxes in indicating glacial productivity levels less than or equal to those of the Holocene. This evidence is consistent with a growing body of evidence for El Niño–like conditions in the eastern equatorial Pacific during the LGM that may have been associated with a southward displacement of the Intertropical Convergence Zone [*Koutavas et al.*, 2002; *Koutavas and Lynch-Stieglitz*, 2003]. Consequently, lower opal burial rates in the EEP during the LGM may be tied to reduced upwelling or to a deeper nutricline.

6.4.3. Changes in Overturning Circulation of Intermediate Waters

[46] The observed changes in opal burial in the equatorial Atlantic and Pacific Oceans could also reflect a fundamental change in the pattern of ocean circulation that ventilates the subtropical thermocline rather than a change in nutrient export from the Southern Ocean, or a change in equatorial upwelling. Water masses upwelling in the equatorial Atlantic and Pacific basins have distinctly different sources, and it is possible that circulation patterns in the SO produce larger pools of available Si in Atlantic or Pacific source waters under certain conditions. Southern source water upwelling in the equatorial Pacific originates for the most part in the Pacific sector of the SO [*Dugdale et al.*, 2002; *Matsumoto et al.*, 2002b; *Toggweiler et al.*, 1991], while southern source water in the equatorial Atlantic originates primarily from the Indian sector of the SO [*Drijfhout et al.*, 2005; *Stramma and England*, 1999; *Stramma and Schott*, 1999], entering through Agulhas retroflection rings into the Benguela Current. The

supply of Agulhas water to the Atlantic is reported to have been reduced substantially during glacial times [*Flores et al.*, 1999; *Franzese et al.*, 2006; *Kuhn and Diekmann*, 2002; *Peeters et al.*, 2004]. Because the Agulhas system and the Drake Passage are the two primary avenues for return flow to the North Atlantic [*Gordon et al.*, 1992], the glacial reduction in supply of Agulhas water may have been compensated by increased supply via the Drake Passage, whether or not there was a net change in the overall overturning circulation of intermediate waters. It is therefore possible that increased Drake Passage input to the Atlantic thermocline could have reduced the supply of dissolved Si to the Pacific thermocline, while increasing the supply of dissolved Si (and possibly other nutrients) to the South Atlantic thermocline, resulting in the observed opposite trends of opal burial in the eastern equatorial Pacific and equatorial Atlantic Oceans. This is highly speculative, but would be an interesting idea to explore using an ocean model with well-resolved nutrient cycles in the SO and the tropics.

7. Conclusions

[47] We conducted a survey of 31 cores spanning the Pacific sector of the Southern Ocean in order to estimate opal fluxes from the last glacial period and the Holocene in a test of the silicic acid leakage hypothesis, which predicts decreased glacial opal burial in the Southern Ocean. Opal fluxes south of the APF were lower during the last glacial period than during the Holocene, while fluxes north of the APF were greater. However, increased fluxes north of the APF were not sufficient to offset decreased fluxes to the south, resulting in a decrease in opal burial in the Pacific sector of the SO during the LGP, equivalent to approximately 15 Gt opal ka^{-1}. This estimate represents the mean weighted average of our entire data set, and it is important to note that bootstrap resampling does not allow us to rule out the null hypothesis that there was no significant difference between Holocene and LGP opal fluxes. This net export of Si from the glacial Southern Ocean is in agreement with previous work [*Chase et al.*, 2003a], and satisfies the primary requirement of the SALH. However, evidence from the tropical oceans does not support certain other predictions of the SALH, namely, that either opal burial or the C_{org}:$CaCO_3$ ratio should have increased in the glacial tropics. The magnitude of changes in tropical opal burial are an order of magnitude smaller than the projected total export of Si from the SO, and are offsetting between the Atlantic and Pacific basins. This suggests that other factors, perhaps changes in upwelling or intermediate water circulation, are likely responsible for observed changes in tropical opal burial during the LGP. Furthermore, our data suggest that there exists an unidentified glacial sink for Si, possibly along the continental margins. This is consistent with a recent revision of the Si budget for the modern ocean [*DeMaster*, 2002], which suggested that opal burial on the margins has been drastically underestimated. The existence of this sink, and its possible effects on glacial CO_2, remain an interesting topic for future investigation. While the absence of evidence in support of the SALH does not constitute ''evidence of absence,'' the sum of paleoevidence to date from the tropical and Southern oceans does not support the predictions of this hypothesis.

[48] **Acknowledgments.** Funding for this research was provided in part by the U.S. NSF (grant OPP02-30268). We thank the core repository at LDEO and the Antarctic Research Facility at FSU for providing samples. Thank you to Mark Siddall and Mary-Elena Carr for helpful discussions and to Peter DeMenocal, Jerry McManus, Doug Martinson, and Katsumi Matsumoto for improving the manuscript through their comments. This is LDEO contribution 7240.

References

Abelmann, A., R. Gersonde, G. Cortese, G. Kuhn, and V. Smetacek (2006), Extensive phytoplankton blooms in the Atlantic sector of the glacial Southern Ocean, *Paleoceanography*, *21*, PA1013, doi:10.1029/2005PA001199.

Abrantes, F. (2000), 200 000 yr diatom records from Atlantic upwelling sites reveal maximum productivity during LGM and a shift in phytoplankton community structure at 18 5000 yr, *Earth Planet. Sci. Lett.*, *176*(1), 7–16, doi:10.1016/S0012-821X(99)00312-X.

Anderson, R. F., and A. P. Fleer (1982), Determination of natural actinides and plutonium in marine particulate material, *Anal. Chem.*, *54*(7), 1142–1147, doi:10.1021/ac00244a030.

Anderson, R. F., M. P. Bacon, and P. G. Brewer (1983a), Removal of ^{230}Th and ^{231}Pa at ocean margins, *Earth Planet. Sci. Lett.*, *66*(1–3), 73–90, doi:10.1016/0012-821X(83)90127-9.

Anderson, R. F., M. P. Bacon, and P. G. Brewer (1983b), Removal of ^{230}Th and ^{231}Pa from the open ocean, *Earth Planet. Sci. Lett.*, *62*(1), 7–23, doi:10.1016/0012-821X(83)90067-5.

Anderson, R. F., Y. Lao, W. S. Broecker, S. E. Trumbore, H. J. Hofmann, and W. Wolfli (1990), Boundary scavenging in the Pacific Ocean: A comparison of ^{10}Be and ^{231}Pa, *Earth Planet. Sci. Lett.*, *96*(3–4), 287–304, doi:10.1016/0012-821X(90)90008-L.

Anderson, R. F., Z. Chase, M. Q. Fleisher, and J. Sachs (2002), The Southern Ocean's biological pump during the Last Glacial Maximum, *Deep Sea Res., Part II*, *49*(9–10), 1909–1938, doi:10.1016/S0967-0645(02)00018-8.

Archer, D., A. Winguth, D. Lea, and N. Mahowald (2000), What caused the glacial/interglacial atmospheric pCO_2 cycles?, *Rev. Geophys.*, *38*(2), 159–189, doi:10.1029/1999RG000066.

Bacon, M. P. (1984), Glacial to interglacial changes in carbonate and clay sedimentation in the Atlantic Ocean estimated from ^{230}Th measurements, *Isot. Geosci.*, *2*(2), 97–111.

Beaufort, L., T. de Garidel-Thoron, A. C. Mix, and N. G. Pisias (2001), ENSO-like forcing on oceanic primary production during the late Pleistocene, *Science*, *293*(5539), 2440–2444, doi:10.1126/science.293.5539.2440.

Beucher, C. P., M. A. Brzezinski, and X. Crosta (2007), Silicic acid dynamics in the glacial sub-Antarctic: Implications for the silicic acid leakage hypothesis, *Global Biogeochem. Cycles*, *21*, GB3015, doi:10.1029/2006GB002746.

Bradtmiller, L. I., R. F. Anderson, M. Q. Fleisher, and L. H. Burckle (2006), Diatom productivity in the equatorial Pacific Ocean from the last glacial period to the present: A test of the silicic acid leakage hypothesis, *Paleoceanography*, *21*, PA4201, doi:10.1029/2006PA001282.

Bradtmiller, L. I., R. F. Anderson, M. Q. Fleisher, and L. H. Burckle (2007), Opal burial in the equatorial Atlantic Ocean over the last 30 ka: Implications for glacial-interglacial changes in the ocean silicon cycle, *Paleoceanography*, *22*, PA4216, doi:10.1029/2007PA001443.

Broecker, W. S., E. Clark, I. Hajdas, and G. Bonani (2004), Glacial ventilation rates for the deep Pacific Ocean, *Paleoceanography*, *19*, PA2002, doi:10.1029/2003PA000974.

Brzezinski, M. A., C. J. Pride, V. M. Franck, D. M. Sigman, J. L. Sarmiento, K. Matsumoto, N. Gruber, G. H. Rau, and K. H. Coale (2002), A switch from $Si(OH)_4$ to NO_3^- depletion in the glacial Southern Ocean, *Geophys. Res. Lett.*, *29*(12), 1564, doi:10.1029/2001GL014349.

Burckle, L. H., and R. W. Burak (1995), Relative abundance of *Eucampia antarctica* as a close proxy to δ^{18}O in upper Quaternary sediments of the Southern Ocean, in *Landscapes and Life: Studies in Honour of Urve Miller*, edited by A. M. Robertsson, pp. 15–22, Cons. de l'Eur., Rixensart, Belgium.

Burckle, L. H., and D. W. Cooke (1983), Late Pleistocene *Eucampia antarctica* abundance stratigraphy in the Atlantic sector of the Southern Ocean, *Micropaleontology*, *29*, 6–10, doi:10.2307/1485648.

Burckle, L. H., D. B. Clarke, and N. J. Shackleton (1978), Isochronous last-abundant-

appearance datum (LAAD) of diatom *Hemidiscus karstenii* in the sub-Antarctic, *Geology*, *6*, 243–246, doi:10.1130/0091-7613(1978)6<243:ILDLOT>2.0.CO;2.

Chase, Z., R. F. Anderson, M. Q. Fleisher, and P. W. Kubik (2002), The influence of particle composition and particle flux on scavenging of Th, Pa and Be in the ocean, *Earth Planet. Sci. Lett.*, *204*(1–2), 215–229, doi:10.1016/S0012-821X(02)00984-6.

Chase, Z., R. F. Anderson, M. Q. Fleisher, and P. W. Kubik (2003a), Accumulation of biogenic and lithogenic material in the Pacific sector of the Southern Ocean during the past 40,000 years, *Deep Sea Res., Part II*, *50*(3–4), 799–832, doi:10.1016/S0967-0645(02)00595-7.

Chase, Z., R. F. Anderson, M. Q. Fleisher, and P. W. Kubik (2003b), Scavenging of ^{230}Th, ^{231}Pa and ^{10}Be in the Southern Ocean (SW Pacific sector): The importance of particle flux, particle composition and advection, *Deep Sea Res., Part II*, *50*(3–4), 739–768, doi:10.1016/S0967-0645(02)00593-3.

CLIMAP project members (1976), The surface of the ice-age Earth, *Science*, *191*(4232), 1131–1137, doi:10.1126/science.191.4232.1131.

De La Rocha, C. L., M. A. Brzezinski, and M. J. DeNiro (1997), Fractionation of silicon isotopes by marine diatoms during biogenic silica formation, *Geochim. Cosmochim. Acta*, *61*(23), 5051–5056, doi:10.1016/S0016-7037(97)00300-1.

De La Rocha, C. L., M. A. Brzezinski, M. J. DeNiro, and A. Shemesh (1998), Silicon-isotope composition of diatoms as an indicator of past oceanic change, *Nature*, *395*(6703), 680–683, doi:10.1038/27174.

DeMaster, D. J. (2002), The accumulation and cycling of biogenic silica in the Southern Ocean: Revisiting the marine silica budget, *Deep Sea Res., Part II*, *49*(16), 3155–3167, doi:10.1016/S0967-0645(02)00076-0.

Dezileau, L., J. L. Reyss, and F. Lemoine (2003), Late Quaternary changes in biogenic opal fluxes in the southern Indian Ocean, *Mar. Geol.*, *202*(3–4), 143–158, doi:10.1016/S0025-3227(03)00283-4.

Diekmann, B. (2007), Sedimentary patterns in the late Quaternary Southern Ocean, *Deep Sea Res., Part II*, *54*(21–22), 2350–2366, doi:10.1016/j.dsr2.2007.07.025.

Drijfhout, S. S., J. Donners, and W. P. M. de Ruijter (2005), The origin of intermediate and subpolar mode waters crossing the Atlantic equator in OCCAM, *Geophys. Res. Lett.*, *32*, L06602, doi:10.1029/2004GL021851.

Dugdale, R. C., and F. P. Wilkerson (1998), Silicate regulation of new production in the equatorial Pacific upwelling, *Nature*, *391*(6664), 270–273, doi:10.1038/34630.

Dugdale, R. C., A. G. Wischmeyer, F. P. Wilkerson, R. T. Barber, F. Chai, M. S. Jiang, and T. H. Peng (2002), Meridional asymmetry of source nutrients to the equatorial Pacific upwelling ecosystem and its potential impact on ocean-atmosphere CO_2 flux: A data and modeling approach, *Deep Sea Res., Part II*, *49*(13–14), 2513–2531, doi:10.1016/S0967-0645(02)00046-2.

Farrell, J. W., T. F. Pedersen, S. E. Calvert, and B. Nielsen (1995), Glacial-interglacial changes in nutrient utilization in the equatorial Pacific Ocean, *Nature*, *377*(6549), 514–517, doi:10.1038/377514a0.

Fleisher, M. Q., and R. F. Anderson (2003), Assessing the collection efficiency of Ross Sea sediment traps using ^{230}Th and ^{231}Pa, *Deep Sea Res., Part II*, *50*(3–4), 693–712, doi:10.1016/S0967-0645(02)00591-X.

Flores, J. A., R. Gersonde, and F. J. Sierro (1999), Pleistocene fluctuations in the Agulhas Current retroflection based on the calcareous plankton record, *Mar. Micropaleontol.*, *37*(1), 1–22, doi:10.1016/S0377-8398(99)00012-2.

Foster, G. L., and D. Vance (2006), Negligible glacial-interglacial variation in continental chemical weathering rates, *Nature*, *444*(7121), 918–921, doi:10.1038/nature05365.

Franck, V. M., M. A. Brzezinski, K. H. Coale, and D. M. Nelson (2000), Iron and silicic acid concentrations regulate Si uptake north and south of the Polar Frontal Zone in the Pacific sector of the Southern Ocean, *Deep Sea Res., Part II*, *47*(15–16), 3315–3338, doi:10.1016/S0967-0645(00)00070-9.

Francois, R., M. P. Bacon, and D. O. Suman (1990), Thorium 230 profiling in deep-sea sediments: High-resolution records of flux and dissolution of carbonate in the equatorial Atlantic during the last 24,000 years, *Paleoceanography*, *5*(5), 761–787.

Francois, R., M. A. Altabet, E. F. Yu, D. M. Sigman, M. P. Bacon, M. Frank, G. Bohrmann, G. Bareille, and L. D. Labeyrie (1997), Contribution of Southern Ocean surface-water stratification to low atmospheric CO_2 concentrations during the last glacial period, *Nature*, *389*(6654), 929–935, doi:10.1038/40073.

Francois, R., M. Frank, M. M. Rutgers van der Loeff, and M. P. Bacon (2004), ^{230}Th normalization: An essential tool for interpreting sedimentary fluxes during the late Quaternary, *Paleoceanography*, *19*, PA1018, doi:10.1029/2003PA000939.

Frank, M., A. Mangini, R. Gersonde, M. Rutgers van der Loeff, and G. Kuhn (1996), Late Quaternary sediment dating and quantification of lateral sediment redistribution applying $^{230}Th_{ex}$: A study from the eastern Atlantic sector of the Southern Ocean, *Geol. Rundsch.*, *85*(3), 554–566, doi:10.1007/BF02369010.

Frank, M., R. Gersonde, M. Rutgers van der Loeff, G. Bohrmann, C. C. Nürnberg, P. W. Kubik, M. Suter, and A. Mangini (2000), Similar glacial and interglacial export bioproductivity in the Atlantic sector of the Southern Ocean: Multiproxy evidence and implications for glacial atmospheric CO_2, *Paleoceanography*, *15*(6), 642–658, doi:10.1029/2000PA000497.

Franzese, A. M., S. R. Hemming, S. L. Goldstein, and R. F. Anderson (2006), Reduced Agulhas leakage during the Last Glacial Maximum inferred from an integrated provenance and flux study, *Earth Planet. Sci. Lett.*, *250*(1–2), 72–88, doi:10.1016/j.epsl.2006.07.002.

Geibert, W., M. M. Rutgers van der Loeff, R. Usbeck, R. Gersonde, G. Kuhn, and J. Seeberg-Elverfeldt (2005), Quantifying the opal belt in the Atlantic and southeast Pacific sector of the Southern Ocean by means of ^{230}Th normalization, *Global Biogeochem. Cycles*, *19*, GB4001, doi:10.1029/2005GB002465.

Gordon, A. L., R. F. Weiss, W. M. Smethie Jr., and M. J. Warner (1992), Thermocline and intermediate water communication between the South Atlantic and Indian oceans, *J. Geophys. Res.*, *97*(C5), 7223–7240, doi:10.1029/92JC00485.

Hammond, D. E., J. McManus, and W. M. Berelson (2004), Oceanic germanium/silicon ratios: Evaluation of the potential overprint of temperature on weathering signals, *Paleoceanography*, *19*, PA2016, doi:10.1029/2003PA000940.

Henderson, G. M., C. Heinze, R. F. Anderson, and A. M. E. Winguth (1999), Global distribution of the ^{230}Th flux to ocean sediments constrained by GCM modelling, *Deep Sea Res., Part I*, *46*(11), 1861–1893, doi:10.1016/S0967-0637(99)00030-8.

Henriksson, A. S. (2000), Coccolithophore response to oceanographic changes in the equatorial Atlantic during the last 200,000 years, *Palaeogeogr. Palaeoclimatol. Palaeoecol.*, *156*(1–2), 161–173, doi:10.1016/S0031-0182(99)00139-X.

Howard, W. R., and W. L. Prell (1992), Late Quaternary surface circulation of the southern Indian Ocean and its relationship to orbital variations, *Paleoceanography*, *7*(1), 79–117, doi:10.1029/91PA02994.

Howard, W. R., and W. L. Prell (1994), Late Quaternary $CaCO_3$ production and preservation in the Southern Ocean: Implications for oceanic and atmospheric carbon cycling, *Paleoceanography*, *9*(3), 453–482, doi:10.1029/93PA03524.

Hurd, D. C., and S. Birdwhistell (1983), On producing a general model for biogenic silica dissolution, *Am. J. Sci.*, *283*, 1–28.

Kamatani, A. (1982), Dissolution rates of silica from diatoms decomposing at various temperatures, *Mar. Biol. Berlin*, *68*, 91–96, doi:10.1007/BF00393146.

Kienast, M., S. S. Kienast, S. E. Calvert, T. I. Eglinton, G. Mollenhauer, R. Francois, and A. C. Mix (2006), Eastern Pacific cooling and Atlantic overturning circulation during the last deglaciation, *Nature*, *443*(7113), 846–849, doi:10.1038/nature05222.

Kienast, S. S., M. Kienast, S. Jaccard, S. E. Calvert, and R. François (2006), Testing the silica leakage hypothesis with sedimentary opal records from the eastern equatorial Pacific over the last 150 kyrs, *Geophys. Res. Lett.*, *33*, L15607, doi:10.1029/2006GL026651.

Koutavas, A., and J. Lynch-Stieglitz (2003), Glacial-interglacial dynamics of the eastern equatorial Pacific cold tongue–Intertropical Convergence Zone system reconstructed from oxygen isotope records, *Paleoceanography*, *18*(4), 1089, doi:10.1029/2003PA000894.

Koutavas, A., J. Lynch-Stieglitz, T. M. Marchitto Jr., and J. P. Sachs (2002), El Niño–like pattern in ice age tropical Pacific sea surface temperature, *Science*, *297*(5579), 226–230, doi:10.1126/science.1072376.

Kuhn, G., and B. Diekmann (2002), Late Quaternary variability of ocean circulation in the southeastern South Atlantic inferred from the terrigenous sediment record of a drift deposit in the southern Cape Basin (ODP Site 1089), *Palaeogeogr. Palaeoclimatol. Palaeoecol.*, *182*(3–4), 287–303, doi:10.1016/S0031-0182(01)00500-4.

Kumar, N., R. F. Anderson, R. A. Mortlock, P. N. Froelich, P. Kubik, B. Dittrichhannen, and M. Suter (1995), Increased biological productivity and export production in the glacial Southern Ocean, *Nature*, *378*(6558), 675–680, doi:10.1038/378675a0.

Lao, Y., R. F. Anderson, W. S. Broecker, S. E. Trumbore, H. J. Hofmann, and W. Wolfli (1992), Transport and burial rates of ^{10}Be and ^{231}Pa in the Pacific Ocean during the Holocene period, *Earth Planet. Sci. Lett.*, *113*(1–2), 173–189, doi:10.1016/0012-821X(92)90218-K.

Lao, Y., R. F. Anderson, W. S. Broecker, H. J. Hofmann, and W. Wolfli (1993), Particulate fluxes of ^{230}Th, ^{231}Pa, and ^{10}Be in the north-

eastern Pacific Ocean, *Geochim. Cosmochim. Acta*, *57*(1), 205–217, doi:10.1016/0016-7037(93)90479-G.

Loubere, P. (2000), Marine control of biological production in the eastern equatorial Pacific Ocean, *Nature*, *406*(6795), 497–500, doi:10.1038/35020041.

Loubere, P., F. Mekik, R. Francois, and S. Pichat (2004), Export fluxes of calcite in the eastern equatorial Pacific from the Last Glacial Maximum to present, *Paleoceanography*, *19*, PA2018, doi:10.1029/2003PA000986.

Lyle, M. (1988), Climatically forced organic-carbon burial in equatorial Atlantic and Pacific oceans, *Nature*, *335*(6190), 529–532, doi:10.1038/335529a0.

Matsumoto, K., J. Lynch-Stieglitz, and R. F. Anderson (2001), Similar glacial and Holocene Southern Ocean hydrography, *Paleoceanography*, *16*(5), 445–454, doi:10.1029/2000PA000549.

Matsumoto, K., T. Oba, J. Lynch-Stieglitz, and H. Yamamoto (2002a), Interior hydrography and circulation of the glacial Pacific Ocean, *Quat. Sci. Rev.*, *21*(14–15), 1693–1704, doi:10.1016/S0277-3791(01)00142-1.

Matsumoto, K., J. L. Sarmiento, and M. A. Brzezinski (2002b), Silicic acid leakage from the Southern Ocean: A possible explanation for glacial atmospheric pCO_2, *Global Biogeochem. Cycles*, *16*(3), 1031, doi:10.1029/2001GB001442.

McIntyre, A., and B. Molfino (1996), Forcing of Atlantic equatorial and subpolar millennial cycles by precession, *Science*, *274*(5294), 1867–1870, doi:10.1126/science.274.5294.1867.

Molfino, B., and A. McIntyre (1990), Precessional forcing of nutricline dynamics in the equatorial Atlantic, *Science*, *249*(4970), 766–769, doi:10.1126/science.249.4970.766.

Mortlock, R. A., and P. N. Froelich (1989), A simple method for the rapid determination of biogenic opal in pelagic marine sediments, *Deep Sea Res., Part A*, *36*(9), 1415–1426, doi:10.1016/0198-0149(89)90092-7.

Nelson, D. M., P. Tréguer, M. A. Brzezinski, A. Leynaert, and B. Quéguiner (1995), Production and dissolution of biogenic silica in the ocean: Revised global estimates, comparison with regional data and relationship to biogenic sedimentation, *Global Biogeochem. Cycles*, *9*(3), 359–372, doi:10.1029/95GB01070.

Nelson, D. M., et al. (2002), Vertical budgets for organic carbon and biogenic silica in the Pacific sector of the Southern Ocean, 1996–1998, *Deep Sea Res., Part II*, *49*(9–10), 1645–1674, doi:10.1016/S0967-0645(02)00005-X.

Orsi, A. H., T. Whitworth, and W. D. Nowlin (1995), On the meridional extent and fronts of the Antarctic Circumpolar Current, *Deep Sea Res., Part I*, *42*(5), 641–673, doi:10.1016/0967-0637(95)00021-W.

Paytan, A., M. Kastner, and F. P. Chavez (1996), Glacial to interglacial fluctuations in productivity in the equatorial Pacific as indicated by marine barite, *Science*, *274*(5291), 1355–1357, doi:10.1126/science.274.5291.1355.

Peacock, S., E. Lane, and J. M. Restrepo (2006), A possible sequence of events for the generalized glacial-interglacial cycle, *Global Biogeochem. Cycles*, *20*, GB2010, doi:10.1029/2005GB002448.

Peeters, F. J. C., R. Acheson, G. J. A. Brummer, W. P. M. de Ruijter, R. R. Schneider, G. M. Ganssen, E. Ufkes, and D. Kroon (2004), Vigorous exchange between the Indian and Atlantic oceans at the end of the past five glacial periods, *Nature*, *430*(7000), 661–665, doi:10.1038/nature02785.

Petit, J. R., et al. (1999), Climate and atmospheric history of the past 420,000 years from the Vostok ice core, Antarctica, *Nature*, *399*(6735), 429–436, doi:10.1038/20859.

Pichat, S., K. W. W. Sims, R. François, J. F. McManus, S. B. Leger, and F. Albarède (2004), Lower export production during glacial periods in the equatorial Pacific derived from $(^{231}Pa/^{230}Th)_{xs,0}$ measurements in deep-sea sediments, *Paleoceanography*, *19*, PA4023, doi:10.1029/2003PA000994.

Pondaven, P., O. Ragueneau, P. Tréguer, A. Hauvespre, L. Dezileau, and J. L. Reyss (2000), Resolving the "opal paradox" in the Southern Ocean, *Nature*, *405*(6783), 168–172, doi:10.1038/35012046.

Sarmiento, J. L., N. Gruber, M. A. Brzezinski, and J. P. Dunne (2004), High-latitude controls of thermocline nutrients and low latitude biological productivity, *Nature*, *427*(6969), 56–60, doi:10.1038/nature02127.

Scholten, J. C., J. Fietzke, S. Vogler, M. M. Rutgers van der Loeff, A. Mangini, W. Koeve, J. Waniek, P. Stoffers, A. Antia, and J. Kuss (2001), Trapping efficiencies of sediment traps from the deep eastern North Atlantic: The ^{230}Th calibration, *Deep Sea Res., Part II*, *48*(10), 2383–2408, doi:10.1016/S0967-0645(00)00176-4.

Scholten, J. C., et al. (2005), Radionuclide fluxes in the Arabian Sea: The role of particle composition, *Earth Planet. Sci. Lett.*, *230*(3–4), 319–337, doi:10.1016/j.epsl.2004.11.003.

Shackleton, N. J. (2000), The 100,000-year ice-age cycle identified and found to lag temperature, carbon dioxide, and orbital eccentricity, *Science*, *289*(5486), 1897–1902, doi:10.1126/science.289.5486.1897.

Siegenthaler, U., et al. (2005), Stable carbon cycle–climate relationship during the late Pleistocene, *Science*, *310*(5752), 1313–1317, doi:10.1126/science.1120130.

Sigman, D. M., and E. A. Boyle (2000), Glacial/interglacial variations in atmospheric carbon dioxide, *Nature*, *407*(6806), 859–869, doi:10.1038/35038000.

Sigman, D. M., M. A. Altabet, D. C. McCorkle, R. Francois, and G. Fischer (1999), The $\delta^{15}N$ of nitrate in the Southern Ocean: Consumption of nitrate in surface waters, *Global Biogeochem. Cycles*, *13*(4), 1149–1166, doi:10.1029/1999GB900038.

Sigmon, D. E., D. M. Nelson, and M. A. Brzezinski (2002), The Si cycle in the Pacific sector of the Southern Ocean: Seasonal diatom production in the surface layer and export to the deep sea, *Deep Sea Res., Part II*, *49*(9–10), 1747–1763, doi:10.1016/S0967-0645(02)00010-3.

Smith, W. O., Jr., R. F. Anderson, J. K. Moore, L. A. Codispoti, and J. M. Morrison (2000), The US Southern Ocean Joint Global Ocean Flux Study: An introduction to AESOPS, *Deep Sea Res., Part II*, *47*(15–16), 3073–3093, doi:10.1016/S0967-0645(00)00059-X.

Stramma, L., and M. England (1999), On the water masses and mean circulation of the South Atlantic Ocean, *J. Geophys. Res.*, *104*(C9), 20,863–20,883, doi:10.1029/1999JC900139.

Stramma, L., and F. Schott (1999), The mean flow field of the tropical Atlantic Ocean, *Deep Sea Res., Part II*, *46*(1–2), 279–303, doi:10.1016/S0967-0645(98)00109-X.

Taguchi, K., K. Harada, and S. Tsunogai (1989), Particulate removal of ^{230}Th and ^{231}Pa in the biologically productive northern North Pacific, *Earth Planet. Sci. Lett.*, *93*(2), 223–232, doi:10.1016/0012-821X(89)90070-8.

Taylor, S. R., and S. M. McLennan (1985), *The Continental Crust: Its Composition and Evolution: An Examination of the Geochemical Record Preserved in Sedimentary Rocks*, 312 pp., Blackwell, Oxford, U. K.

Toggweiler, J. R., K. Dixon, and W. S. Broecker (1991), The Peru upwelling and the ventilation of the South Pacific thermocline, *J. Geophys. Res.*, *96*(C11), 20,467–20,497, doi:10.1029/91JC02063.

Tréguer, P., D. M. Nelson, A. J. Van Bennekom, D. J. DeMaster, A. Leynaert, and B. Quéguiner (1995), The silica balance in the world ocean: A reestimate, *Science*, *268*(5209), 375–379, doi:10.1126/science.268.5209.375.

Trull, T., S. R. Rintoul, M. Hadfield, and E. R. Abraham (2001), Circulation and seasonal evolution of polar waters south of Australia: Implications for iron fertilization of the Southern Ocean, *Deep Sea Res., Part II*, *48*(11–12), 2439–2466, doi:10.1016/S0967-0645(01)00003-0.

Valdes, P. J. (2000), South American palaeoclimate model simulations: How reliable are the models?, *J. Quat. Sci.*, *15*(4), 357–368, doi:10.1002/1099-1417(200005)15:4<357::AID-JQS547>3.0.CO;2-8.

Verardo, D. J., and A. McIntyre (1994), Production and destruction: Control of biogenous sedimentation in the tropical Atlantic 0–300,000 years B.P., *Paleoceanography*, *9*(1), 63–86, doi:10.1029/93PA02901.

Walter, H. J., M. M. Rutgers van der Loeff, and H. Hoeltzen (1997), Enhanced scavenging of ^{231}Pa relative to ^{230}Th in the South Atlantic south of the polar front: Implications for the use of the $^{231}Pa/^{230}Th$ ratio as a paleoproductivity proxy, *Earth Planet. Sci. Lett.*, *149*(1–4), 85–100, doi:10.1016/S0012-821X(97)00068-X.

Warnock, J., R. Scherer, and P. Loubere (2007), A quantitative assessment of diatom dissolution and late Quaternary primary productivity in the eastern equatorial Pacific, *Deep Sea Res., Part II*, *54*(5–7), 772–783, doi:10.1016/j.dsr2.2007.01.011.

Yu, E.-F., R. Francois, M. P. Bacon, and A. P. Fleer (2001), Fluxes of ^{230}Th and ^{231}Pa to the deep sea: Implications for the interpretation of excess ^{230}Th and $^{231}Pa/^{230}Th$ profiles in sediments, *Earth Planet. Sci. Lett.*, *191*(3–4), 219–230, doi:10.1016/S0012-821X(01)00410-1.

R. F. Anderson, L. H. Burckle, and M. Q. Fleisher, Lamont-Doherty Earth Observatory of Columbia University, Palisades, NY 10964, USA.

L. I. Bradtmiller, Department of Marine Chemistry and Geochemistry, Woods Hole Oceanographic Institution, Woods Hole, MA 02543, USA. (lbradtmiller@whoi.edu)